Extension of Poincaré's program for integrability, chaos and bifurcations

Ferdinand Verhulst

Mathematisch Instituut
University of Utrecht, PO Box 80.010, 3508 TA Utrecht, The Netherlands
(E-mail: f.verhulst@uu.nl)

Abstract. We will review the achievements of Henri Poincaré in the theory of dynamical systems and will add a number of extensions and generalizations of his results. It is pointed out that the attention given to two degrees-of-freedom Hamiltonian systems is rather deceptive as near stable equilibrium such systems play a special part. We illustrate Poincaré's theory of critical exponents for the Hamiltonian (1 : 2 : 2)-resonance. To assess the measures of chaos, asymptotic estimates in terms of magnitude and timescales can be given. Another of Poincaré's topic, bifurcations, is briefly reviewed.
Keywords: Henri Poincaré, Critical exponents, Asymptotic integrability, Bifurcations.

1 Key results of Poincaré

Received: 20 September 2011 / Accepted: 21 October 2011

ISSN 2241-0503

We restrict ourselves to a discussion of the 'Méthodes nouvelles de la mécanique célèste' (based on [17]), leaving aside for instance the interesting thesis and the Mémoire on differential equations. The following key results are in the field of dynamical systems, the chapter indication refers to the 'Méthodes nouvelles':

- Poincaré-expansion with respect to a small parameter around a particular solution of a differential equation (chapter 2).
- The Poincaré-Lindstedt expansion method (chapter 3) as continuation method and as bifurcation method for periodic solutions.
- Characteristic exponents and expansion of exponents in the presence of a small parameter; exponents when first integrals exist (chapter 4).
- The famous proof that in general for time-independent Hamiltonian systems no other first integrals exist besides the energy (chapter 5).
- The idea of 'asymptotic series' as opposed to convergent series (chapters 7 and 8).
- The divergence of series expansions in celestial mechanics (chapters 9 and 13).
- The Poincaré-domain to characterise resonance in normal forms (chapter 13 and in his thesis).
- The notion of 'asymptotic invariant manifold' (chapter 25).
- The recurrence theorem (chapter 26).
- The Poincaré-map as a tool for dynamical systems (chapter 27).
- Homoclinic (doubly asymptotic) and heteroclinic solutions; the image of the corresponding orbit structure.

The term 'New methods' contrasts with the old methods of Lagrange, Laplace, Delaunay, Jacobi that are correct and classical, but leaving a great many unsolved problems. This holds in particular for integrability questions, convergence of series which is related to Poisson-stability and bifurcation theory.

2 The deception of two degrees-of-freedom

A time-independent Hamiltonian produces equations of motion that have in general only one first integral, the energy. So, for integrability of a two d-o-f Hamiltonian system, a second independent integral is needed, but near stable equilibrium both numerics and analytic approximation suggests integrability in this case. Why?

The reason is, that the measure of chaos in two d-o-f near stable equilibrium is exponentially small. We will discuss this in more detail in section four. A famous example is the Hénon-Heiles problem [6] that was published in 1964. For small values of the energy it looks integrable and many futile expansions were computed to pinpoint this apparent second integral. The 'proofs'were futile, but as we shall see, such expansions are not useless. For small values of the energy they describe the KAM-tori that abound near stable equilibrium of near-integrable systems.

The dynamics of a time-independent Hamiltonian system corresponds with a two-dimensional area-preserving Poincaré-map. We can turn this around:

a two-dimensional area-preserving map has a suspension that is Hamiltonian. Consider as an example a two-dimensional area-preserving map T_H studied by Igor Hoveijn [9]:

$$\begin{pmatrix} x \\ y \end{pmatrix} \to \begin{pmatrix} \cos\alpha & -\sin\alpha \\ \sin\alpha & \cos\alpha \end{pmatrix} \begin{pmatrix} x \\ y \end{pmatrix} + \sin x \begin{pmatrix} -\sin\alpha \\ \cos\alpha \end{pmatrix}. \tag{1}$$

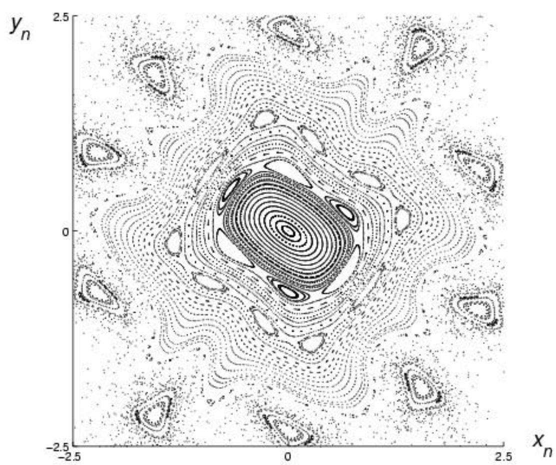

Fig. 1. The area-preserving map T_H produced by eq. (1) for $\alpha = 3\pi/5$. In the centre of the plane there is a dominant family of closed KAM-curves. In between the curves there are again stable and unstable periodic solutions but they can not be observed at this level of precision. Outside this family of closed curves one finds stable periodic solutions associated with unstable periodic solutions. Moving out one observes a stable and unstable 10-periodic solution and further on another pair of 10-periodic solutions. The unstable solutions have stable and unstable manifolds that intersect an infinite number of times producing chaotic behaviour. The dots correspond with orbits returning chaotically in the plane when applying the map repeatedly. Poincaré described the folding process, see [17], that can be seen dynamically by considering a small square in the plane and following its subsequent mappings (figure courtesy Igor Hoveijn).

In fig. 1 we took $\alpha = 3\pi/5$. The closed KAM-curves around the centre suggest that for small values of x and y the map is nearly integrable. For larger values of x and y the chaotic nature of the map becomes more transparent.

3 Critical exponents, the (1 : 2 : 2)-resonance

Chapter four of the 'Méthodes nouvelles' introduces characteristic exponents. Consider an n-dimensional autonomous equation of the form

$$\dot{x} = X(x),$$

and suppose we know a particular solution $x = \phi(t)$. We call this a generating solution. When studying neighbouring solutions of $\phi(t)$ we put

$$x = \phi(t) + \xi.$$

The variational equations of $\phi(t)$ are obtained by substituting $x = \phi(t) + \xi$ into the differential equation and linearising for small ξ to obtain

$$\dot{\xi} = \frac{\partial X}{\partial x}|_{x=\phi(t)}\xi.$$

If $\phi(t)$ is a periodic solution, the variational equations are a Floquet system.

Using the variational equations we can obtain a linear system of equations of which the characteristic eigenvalue equation produces the characteristic exponents. There are some important cases:

- It is clear from the linear system determining the characteristic exponents that if $X(x,t)$ does not depend explicitly on t, the autonomous case, $\dot{\phi}(t)$ is a solution, so one of the characteristic exponents is zero.
- If the vector field is time-dependent ($\dot{x} = X(x,t)$) and contains a small parameter μ, can be expanded with respect to this parameter and admits a T-periodic solution $\phi(t)$ for $\mu = 0$, a periodic solution for small nonzero values of μ exists if all the characteristic exponents of $\phi(t)$ are nonzero.
- If the vector field X is autonomous, has a periodic solution and we have one and only one zero characteristic exponent, the same conclusion for the existence of a periodic solution holds.
- If we have a T-periodic equation of $\dot{x} = X(x,t)$ with T-periodic solution $\phi(t)$ and in addition an analytic first integral $F(x) =$ constant, at least one of the characteristic exponents of $\phi(t)$ is zero; the rather exceptional case for this result is if all the partial derivatives $\partial F/\partial x$ vanish for $x = \phi(t)$.
- If the vector field X is autonomous and we have p independent first integrals, $p < n$, we have at least $p + 1$ characteristic exponents zero.

A number of special results hold in the case that our nonlinear system of differential equations is Hamiltonian and autonomous. Poincaré proves, that in this case the $2n$ characteristic exponents of a periodic solution, emerge in pairs $\lambda_i, -\lambda_i$, equal in size and of opposite sign. In addition, the energy integral produces two characteristic exponents zero; if there exist p other independent first integrals we have either $2p + 2$ characteristic exponents zero or, in the exceptional case, the functional determinants of the integrals restricted to the periodic solution vanish. For the proof, Poincaré uses Poisson brackets and the theory of independent solutions of linear systems.

If the time-independent Hamiltonian system has a periodic solution with more than two zero characteristic exponents, this can be caused by the presence of another first integral besides the energy or it may be the exceptional case.

Examples of more than two zero characteristic exponents are found in the normal forms of three degrees-of-freedom systems in $1 : 2 : n$-resonance with $n > 4$, where normalization to H_3 produces two families of periodic solutions on the energy manifold. The normal form truncated to cubic terms is integrable. The families break up when adding higher order normal form terms; see [13]. The technical problems connected with drawing conclusions from the presence of more than two zero characteristic exponents, have probably prevented its use in research of conservative dynamics, but the statement "a continuous family of periodic solutions on the energy manifold is a non-generic phenomenon" is one of the remaining features in the literature. Nowadays the analysis is easier by the use of numerical continuation methods.

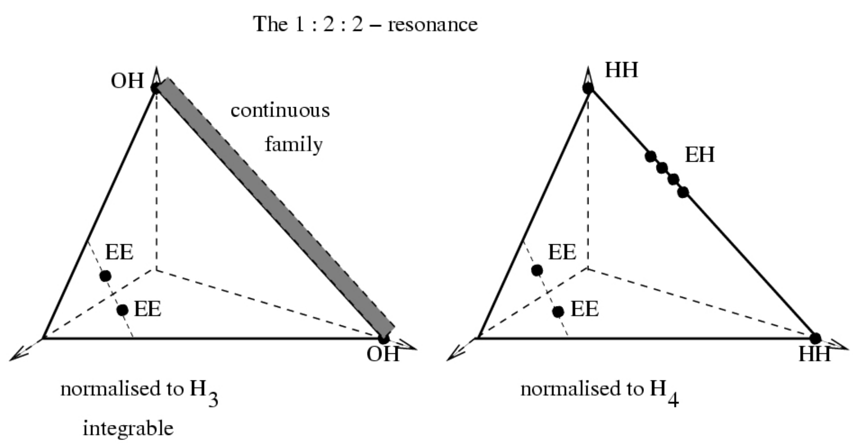

Fig. 2. The three d-o-f (1 : 2 : 2)-Hamiltonian resonance, left the periodic solutions in an action simplex of the Hamiltonian normlised to H_3, right normalization to H_4 (figure courtesy Springer).

Regarding the complications it is of interest to look at the general (1 : 2 : 2)-resonance, see fig. 2. The general Hamiltonian has 56 cubic terms, normalization leaves three cubic terms. Remarkably enough, the cubic normal form is integrable with energy integral, a quadratic integral and a cubic integral. However, on the energy manifold we find one continuous family of periodic solutions and two isolated solutions. So we have here an exceptional case as described by Poincaré. It turns out that the cubic normal form displays a hidden symmetry that vanishes at higher order. The interpretation is that the phase-flow shows this symmetry with accuracy $O(\varepsilon)$ on the timescale $1/\varepsilon$, the integrability is asymptotic with error estimate $O(\varepsilon^2 t)$ (see the next section for the error estimates). In fig. 2 the action simplex of the normal form to H_4 (before normalization 126 terms) shows the break-up of the continuous family of periodic solutions into six periodic solutions on the energy manifold.

4 Measures of chaos

Most Hamiltonian systems are not integrable. However, as we shall see, this is a very deceptive statement although it is mathematically correct. To get

this in the right perspective, we shall start by outlining suitable approximation methods. These are canonical normal form methods, sometimes called after Birkhoff-Gustavson, and averaging performed in a canonical way. The methods admit precise error estimates and enable us therefore to determine local measures of regularity and chaos. The methods also permit us to locate normal modes and other short-periodic solutions.
We recall that two d-o-f time-independent Hamiltonian systems near stable equilibrium can be normalized and that the normal form is always integrable to any order. The integrals are the Hamiltonian and its quadratic part. The motion on the KAM-tori dominates phase-space and this result expresses that the amount of chaos near stable equilibrium is exponentially small. Explicitly: near stable equilibrium, the measure of chaos is $O(\varepsilon^a \exp(-1/\varepsilon^b)$ for suitable positive constants a, b where the energy $E = O(\varepsilon^2)$. An illustrative example is studied in [7].

4.1 Approximations and normal forms

Consider the n degrees of freedom time-independent Hamiltonian

$$H(p,q) = \frac{1}{2}\sum_{i=1}^{n} \omega_i \left(p_i^2 + q_i^2\right) + H_3 + H_4 + \cdots . \tag{2}$$

with H_k, $k \geq 3$ a homogeneous polynomial of degree k and positive frequencies ω_i. We introduce a small parameter ε into the system by rescaling the variables by $q_i = \varepsilon \overline{q_i}, p_i = \varepsilon \overline{p_i}, i = 1, \cdots, n$ and dividing the Hamiltonian by ε^2. This implies that we localize near stable equilibrium with energy $O(\varepsilon^2)$.
We can define successive, nonlinear coordinate (or *near-identity*) transformations that will bring the Hamiltonian into the so-called Birkhoff normal form; see [3] and [14] for details and references. For a general dynamical systems reference see [1,4], for symmetry in the context of Hamiltonian systems see [4,10]. A stimulating text on chaos and resonance is [5]. In action-angle variables τ, ϕ, a Hamiltonian H is said to be in Birkhoff normal form of degree $2k$ if it can be written as

$$H = \sum_{i=1}^{n} \omega_i \tau_i + \varepsilon^2 P_2(\tau) + \varepsilon^4 P_3(\tau) + \cdots + \varepsilon^{2k-2} P_k(\tau),$$

where $\tau = (\tau_1, \cdots, \tau_n)$ and $P_i(\tau)$ is a homogeneous polynomial of degree i in $\tau_i = \frac{1}{2}({p_i}^2 + {q_i}^2), i = 1, \cdots, n$. The variables τ_i are called actions; note that if Birkhoff normalization is possible, the angles have been eliminated. If a Hamiltonian can be transformed into Birkhoff normal form, the dynamics is fairly regular. The system is integrable with integral manifolds which are tori described by taking τ_i constant. The flow on the tori is quasi-periodic.
Suppose a Hamiltonian is in Birkhoff normal form to degree m, but the frequencies are satisfying a resonance relation of order $m + 1$. This means that H_{m+1}, H_{m+2} etc. may contain resonant terms which can not be transformed away. The procedure is now to split H_{m+1}, H_{m+2} etc. in resonant terms and

terms to which the Birkhoff normalization process can be applied. The resulting normal form will generally contain resonant terms and is called Birkhoff-Gustavson normal form. It contains terms dependent on the action τ and on resonant combination angles of the form $\chi_i = k_1\phi_1 + \cdots + k_n\phi_n$. In practice we have to consider a truncation of the Birkhoff-Gustavson normal form $\bar{H}$ at some degree $p \geq m$:

$$\bar{H} = H_2 + \varepsilon\bar{H}_3 + \varepsilon^2\bar{H}_4 + \cdots + \varepsilon^{p-2}\bar{H}_p. \tag{3}$$

Because of the construction we have the following results:

- $\bar{H}$ is conserved for the original Hamiltonian system (2) with error $O(\varepsilon^{p-1})$ for all time.
- H_2 is conserved for the original Hamiltonian system (2) with error $O(\varepsilon)$ for all time. So the normal form has at least two integrals. Symmetry can enhance the regularity, see [13].
- If we find other integrals of the Birkhoff-Gustavson normal form, we have slightly weaker error estimates. Explicitly, suppose that $F(p,q)$ is an independent integral of the truncated Hamiltonian system (3), we have for the solutions of the original Hamiltonian system (2) the estimate

$$F(p,q) - F(p(0), q(0)) = O(\varepsilon^{p-1}t).$$

An important consequence is the following statement: if the phaseflow induced by the truncated Hamiltonian (3) is completely integrable, the flow of the original Hamiltonian (2) is approximately integrable or asymptotically integrable in the sense described above. In this case the original system is called *formally integrable*. This implies that the irregular, chaotic component in the flow of the original Hamiltonian is limited by the given error estimates and must be a small-scale phenomenon on a long timescale. For details see [14] and [13].

4.2 Normal modes and short-periodic solutions

Liapunov proved that if the frequencies ω_i satisfy no resonance relation, the normal modes, obtained by linearization, can be continued for the full, nonlinear Hamiltonian system (2), resulting in at least n short-periodic solutions with periods ε-close to $2\pi/\omega_i$.

Weinstein [18] proved that even in the case of resonance, there exist at least n short-periodic solutions of Hamiltonian system (2). Note, that these periodic solutions are not necessarily continuations of the linear modes, the term 'normal modes' in this context can be confusing. Another important point is that n short-periodic solutions is really the minimum number. For instance in the case of two degrees of freedom, 2 short-periodic solutions are guaranteed to exist by the Weinstein theorem. But in the $1:2$ resonance case one finds generically 3 short-periodic solutions for each (small) value of the energy. One of these is a continuation of a linear normal mode, the other two are not. For higher-order resonances like $3:7$ or $2:11$, there exist for an open set of parameters four short-periodic solutions of which two are continuations of the normal modes.

Of course symmetry and special Hamiltonian examples may change this picture drastically.

4.3 Three degrees of freedom

The question of asymptotic integrability is different for more than two degrees of freedom. First we consider the genuine first order resonances of three d-o-f systems.

First-order resonances

As we have seen, the cubic normal form of the $(1:2:2)$-resonance is integrable; this is caused by a hidden symmetry which reveals itself by normalization. The $(1:2:1)$-resonance and the $(1:2:3)$-resonance on the other hand are not integrable for an open set of parameters of the Hamiltonian. The results are illustrated for the four first-order resonances in the table from [13].
If three independent integrals of the normalized system can be found, the normalized system is integrable. The integrability depends in principle on how far the normalization is carried out ($\overline{H}_k$ represents the normal form of H_k, the homogeneous part of the Hamiltonian of degree k). The formal integrals have a precise asymptotic meaning as discussed in section 4.1. We use the following abbreviations: *no cubic integral* for no quadratic or cubic third integral; *discr. symm.* q_i for discrete (or mirror) symmetry in the p_i, q_i-degree of freedom; *2 subsystems at* $\overline{H}_k$ for the case that the normalized system decouples into a one and a two degrees of freedom subsystem upon normalizing to H_k. In the second and third column one finds the number of known integrals when normalizing to $\overline{H}_3$ respectively $\overline{H}_4$.

The remarks which have been added to the table reflect some of the results known on the non-existence of third integrals. Note that the results presented here are for the general Hamiltonian and that additional assumptions, in particular involving symmetry, may change the results. In this respect it is interesting that in a number of applications, chaotic dynamics appears to be of relatively small size. An example is the dynamics of elliptical galaxies that display three-axial symmetry. Astrophysical observations suggest highly nonlinear but integrable motion. The statements above with indication 'Assumptions': 'general', are for Hamiltonian systems in general form near stable equilibrium.

Example: the $(1:2:3)$*-resonance*

This resonance was analyzed in [8] and [15]. We will summarize some results and formulate some open problems. When normalizing to H_4 one finds 7 short-periodic (families of) solutions. One of them is for an open set of parameters complex unstable (for the complementary set it is unstable of saddle type). This complex instability is a source of chaotic behaviour. Using Šilnikov-Devaney theory, it is shown in [8] that a horseshoe map exists in the normal form to H_4 which makes the normal form chaotic.
Numerics indicate that the normal form $\bar{H} = H_2 + \bar{H}_3$ is already chaotic, but a proof is missing. Also the dynamics of the case where the periodic solution is unstable, but of saddle type, has still to be characterized.
Discrete symmetry in either the first or the last degree of freedom makes the normal form to H_4 integrable.

Table 1. Integrability of the normal forms of the four genuine first order resonances.

Resonance	Assumptions	H_3	H_4	Remarks
1:2:1	general	2	2	no analytic third integral
	discr.symm. q_1	2	2	no analytic third integral
	discr.symm. q_2	3	3	$\overline{H}_3 = 0$; 2 subsystems at $\overline{H}_4$
	discr.symm. q_3	2	2	no analytic third integral
1:2:2	general	3	2	no cubic third integral at $\overline{H}_4$
	discr.symm. q_2 and q_3	3	3	$\overline{H}_3 = 0$; 2 subsystems at $\overline{H}_4$
1:2:3	general	2	2	no analytic third integral
	discr.symm. q_1	3	3	2 subsystems at $\overline{H}_3$ and $\overline{H}_4$
	discr.symm. q_2	3	3	$\overline{H}_3 = 0$
	discr.symm. q_3	3	3	2 subsystems at $\overline{H}_3$ and $\overline{H}_4$
1:2:4	general	2	2	no cubic third integral
	discr.symm. q_1	2	2	no cubic third integral
	discr.symm. q_2 or q_3	3	3	2 subsystems at $\overline{H}_3$ and $\overline{H}_4$

Higher-order resonances

Higher order resonances abound in applications. The results discussed thus far are mostly general, but, with regards to applications, it is very important to look again at the part played by symmetries. This will be illustrated for the $(1 : 3 : 7)$-resonance and will be discussed in some detail. This also serves as an example that resonances with odd resonance numbers are particularly sensitive to symmetries.

Example: the $(1 : 3 : 7)$*-resonance*

We start with the general Hamiltonian with this resonance in H_2:

$$H_2 = \tau_1 + 3\tau_2 + 7\tau_3.$$

At H_3 level there is no resonance and we find after normalization, $\bar{H}_3 = 0$. There are two combination angles active at H_4 level:

$$\chi_1 = 3\phi_1 - \phi_2 \text{ and } \chi_2 = \phi_1 + 2\phi_2 - \phi_3.$$

At H_5 level no combination angles are added, H_5 can be brought in Birkhoff normal form. We list the consequences of mirror symmetry in each respective degree of freedom:

- In the first d-o-f: χ_1 and χ_2 not active; formal integrability until $\bar{H}_5$, chaotic dynamics has measure $O(\varepsilon^4 t)$.
- In the second d-o-f: χ_1 not active; formal integrability until $\bar{H}_7$, chaotic dynamics has measure $O(\varepsilon^6 t)$.
- In the third d-o-f: χ_2 not active; formal integrability until $\bar{H}_7$, chaotic dynamics has measure $O(\varepsilon^6 t)$.
- The case of mirror symmetry in all three d-o-f. is discussed below.

One can continue the analysis to higher order normal forms to obtain more precise estimates of the remaining chaotic dynamics. We discuss an example.

Three-axial elliptical galaxies in $(1:3:7)$*-resonance*
In this case we have discrete (mirror) symmetry in three degrees of freedom. Until H_7 the system can be brought into Birkhoff normal form, chaotic dynamics has measure $O(\varepsilon^6 t)$ which predicts regular behaviour on a long timescale. The Birkhoff-Gustavson normal form $\bar{H}_8$ contains the combination angles $6\phi_1 - 2\phi_2$ and $2\phi_1 + 4\phi_2 - 2\phi_3$.
The situation needs a very high degree of normalization as becomes clear when considering the analysis of periodic solutions. Because of the discrete symmetry $\tau_i = 0, i = 1, 2, 3$ each corresponds with a two d-o-f submanifold of the original (symmetric) Hamiltonian. The normal modes are exact periodic solutions of the normal form and the original Hamiltonian. The normal forms in these 4-dimensional submanifolds are all integrable (section 4.1) and chaotic behaviour takes place in exponentially small sets. Consider the question of how far we have at least to normalize the flow in these submanifolds.
Case $\tau_1 = 0$. This is the worst case, as it involves the $3:7$-resonance. In the symmetric case this system has to be normalized to H_{20} to characterize the periodic solutions.
Case $\tau_2 = 0$ involving the $1:7$-resonance. The system has to be normalized to H_{16} to characterize the periodic solutions.
Case $\tau_3 = 0$ involving the $1:3$-resonance. This relatively well-known system has to be normalized to H_8 to characterize the periodic solutions. In [13] it is described how to deal with such higher-order cases.

4.4 A remark on chains of oscillators

Our knowledge of chains of oscillators is still restricted. Remarkably enough the normal form of the $1:2:\cdots:2$-resonance with n degrees of freedom is integrable. Consider the Hamiltonian

$$H(p,q) = \frac{1}{2}(p_1^2 + q_1^2) + \sum_{i=2}^{n}(p_i^2 + q_i^2) + H_3 + \cdots,$$

where $H_3 + \cdots$ represents the general cubic and higher order terms. The Hamiltonian is formally integrable and the proof runs along the lines of the analysis of the $(1:2:2)$-resonance, displaying again hidden symmetry.
A spectacular result arises for the classical Fermi-Pasta-Ulam problem which is a chain of identical oscillators coupled by nearest neighbour interaction. At low energy levels the chain shows recurrence and no chaos. Recently it was shown in [12] by normal form methods and symmetry considerations, that a nearby integrable system exists which make the KAM-theorem applicable. This solves the recurrence phenomenon at low energy.

5 Bifurcations

The analysis of periodic solutions is based on the implicit function theorem. If the conditions of the theorem are not satisfied we have a *bifurcation*.

The treatment in the 'Méthodes nouvelles' is very general, it applies to nonlinear ODEs, including dissipative systems. The bifurcations discussed have a universal character:

- Hopf bifurcation (continuation near an equilibrium).
- Transcritical bifurcation, exchange of stability.
- Emergence and vanishing of periodic solutions in pairs.

A bifurcation that plays a very prominent role in nonlinear dynamics is the Hopf bifurcation, also referred to as Poincaré-Andronov-Hopf bifurcation. It may happen that, when an equilibrium point of which the eigenvalues depend on parameters, will have two purely imaginary eigenvalues if one of the parameters (μ) assumes a critical value, say μ_0. In this case, depending on the nonlinearities, there may exist a nearby periodic solution. If the periodic solution emerges for $\mu < \mu_0$ it is called subcritical, for $\mu > \mu_0$ it is supercritical.

For periodic solutions and fixed points of a map, there are analogous results, where one usually refers to generalized Hopf, Hopf-Hopf or Neimark-Sacker bifurcation.

The first place where the Hopf bifurcation arises in the literature is in the Méthodes nouvelles. Poincaré considers an equilibrium of an autonomous equation in R^n

$$\dot{x} = X(x)$$

and views this equilibrium as a periodic solution with arbitrary period. Suppose that there is a parameter μ in the equation and that $x_1 = x_2 = \cdots = x_n = 0$ is an equilibrium for any value of μ. We will look for a periodic solution near the origin $x = 0$ for $\mu = 0$, with initial value $x(0) = \beta$ and $x(T) = \psi + \beta$. If we can determine T with $\psi = 0$ and non-trivial β, we have found a periodic solution. Poincaré finds from the determinant of the Jacobian J:

$$J = \frac{\partial X}{\partial x}|_{\mu=0,x=0},$$

that if $|J| \neq 0$, we will have only the trivial solution $\beta = 0$, corresponding with the equilibrium solution $x = 0$. The condition $|J| = 0$ to obtain a nontrivial solution corresponds with (at least) two eigenvalues to be purely imaginary and conjugate. This condition makes the existence of a small periodic solution branching off equilibrium $x = 0$ possible, but we still have to consider the nonlinear terms to see whether a periodic solution actually emerges.

The eigenvalues λ_i will depend on μ. Adding the condition that at the critical value $\mu_0 = 0$, we have two conjugate imaginary eigenvalues $\lambda_{i,j}$ with $d\lambda_{i,j}/d\mu \neq 0$, we will call such a bifurcation value of μ a Hopf point.

Poincaré considers in the 'Méthodes nouvelles' as an example the equations formulated by Hill for the motion of the Moon, two second-order equations with one nontrivial equilibrium. The equilibrium corresponds with the Moon being in constant conjunction or opposition at constant distance of the Earth. The eigenvalues of the Jacobian as formulated above, have two real values and two conjugate imaginary ones. The conclusion is that a periodic solution exists near this equilibrium in near-opposition or near-conjunction with an amplitude that grows with the small parameter $\sqrt{\mu}$. As two conjugate eigenvalues are real, it will be unstable.

The classical example of the Van der Pol-equation is easier to analyse. Poincaré's interest in wireless telegraphy induced him to use periodic solutions obtained by this type of bifurcation, see [17].

5.1 Tori created by Neimark-Sacker bifurcation

Another important scenario to create a torus, arises from the Neimark-Sacker bifurcation. For an instructive and detailed introduction see Kuznetsov (2004) [11]. Suppose that we have obtained an averaged equation $\dot{x} = \varepsilon f(x, a)$, with dimension 3 or higher, by variation of constants and subsequent averaging; a is a parameter or a set of parameters. It is well-known that if this equation contains a hyperbolic critical point, the original equation contains a periodic solution. The first order approximation of this periodic solution is characterized by the time variables t and εt.
Suppose now that by varying the parameter a a pair of eigenvalues of the critical point becomes purely imaginary. For this value of a the averaged equation undergoes a Hopf bifurcation producing a periodic solution of the averaged equation; the typical time variable of this periodic solution is εt and so the period will be $O(1/\varepsilon)$. As it branches off an existing periodic solution in the original equation, it will produce a torus; it is associated with a Hopf bifurcation of the corresponding Poincaré map and the bifurcation has a different name: Neimark-Sacker bifurcation. The result will be a two-dimensional torus which contains two-frequency oscillations, one on a timescale of order 1 and the other with timescale $O(1/\varepsilon)$.

A special case of a system studied by Bakri et al. (2004) [2] is:

$$\begin{aligned} \ddot{x} + \varepsilon\kappa\dot{x} + (1 + \varepsilon\cos 2t)x + \varepsilon xy &= 0, \\ \ddot{y} + \varepsilon\dot{y} + 4(1+\varepsilon)y - \varepsilon x^2 &= 0. \end{aligned}$$

This is a system with parametric excitation and nonlinear coupling; κ is a positive damping coefficient which is independent of ε. Away from the coordinate planes we may use amplitude-phase variables by $x = r_1\cos(t+\psi_1), \dot{x} = -r_1\sin(t+\psi_1), y = r_2\cos(2t+\psi_2), \dot{y} = -2r_2\sin(2t+\psi_1)$; after first order averaging we find, omitting the subscripts a, the system

$$\begin{aligned} \dot{r}_1 &= \varepsilon r_1(\frac{r_2}{4}\sin(2\psi_1-\psi_2) + \frac{1}{4}\sin 2\psi_1 - \frac{1}{2}\kappa), \\ \dot{\psi}_1 &= \varepsilon(\frac{r_2}{4}\cos(2\psi_1-\psi_2) + \frac{1}{4}\cos 2\psi_1), \\ \dot{r}_2 &= \varepsilon\frac{r_2}{2}(\frac{r_1^2}{4r_2}\sin(2\psi_1-\psi_2) - 1), \\ \dot{\psi}_2 &= \frac{\varepsilon}{2}(-\frac{r_1^2}{4r_2}\cos(2\psi_1-\psi_2) + 2). \end{aligned}$$

Putting the righthand sides equal to zero produces a nontrivial critical point corresponding with a periodic solution of the system for the amplitudes and phases and so a quasi-periodic solution of the original coupled system in x and y. We find for this critical point the relations

$$r_1^2 = 4\sqrt{5}r_2, \cos(2\psi_1 - \psi_2) = \frac{2}{\sqrt{5}}, \sin(2\psi_1 - \psi_2) = \frac{1}{\sqrt{5}}, r_1 = 2\sqrt{2\kappa + \sqrt{5 - 16\kappa^2}}.$$

This periodic solution exists if the damping coefficient is not too large: $0 \leq \kappa < \frac{\sqrt{5}}{4}$. Linearization of the averaged equations at the critical point while using these relations produces a (4×4) matrix A.

A condition for the existence of the periodic solution is that the critical point is hyperbolic, i.e. the eigenvalues of the matrix A have no real part zero. It is possible to express the eigenvalues explicitly in terms of κ by using a software package like MATHEMATICA. However, the expressions are cumbersome. Hyperbolicity is the case if we start with values of κ just below $\frac{\sqrt{5}}{4} = 0.559$. Diminishing κ we find that, when $\kappa = 0.546$, the real part of two eigenvalues vanishes. This value corresponds with a Hopf bifurcation producing a nonconstant periodic solution of the averaged equations. This in its turn corresponds with a torus in the original equations (in x and y) by a Neimark-Sacker bifurcation. As stated before, the result will be a two-dimensional torus which contains two-frequency oscillations, one on a timescale of order 1 and the other with timescale $O(1/\varepsilon)$.

6 Breakdown and bifurcations of tori

Complementary to the emergence of tori, their breakdown is of great theoretical and practical interest. In particular we would like to have a general idea of how two-dimensional invariant tori break down and how nontrivial limit sets are created when certain parameters are varied. To obtain insight the analysis of maps can be very helpful as the phenomena governed by differential equations are much more implicit.

A common feature is the presence of stable and unstable periodic solutions in p/q-resonance on a torus. Breakup can be triggered by heteroclinic tangencies, arising when a parameter is varied. This leads rather quickly to strange, chaotic behaviour. There are other scenarios producing strange behaviour where the normal hyperbolicity of the torus decreases more gradually. For an introduction and references see [16].

References

1.Arnol'd, V.I., *Mathematical Methods of Classical Mechanics*, Springer-Verlag, New York etc., 1978.

2.Bakri, T., Nabergoj, R., Tondl, A., Verhulst, F. *Parametric excitation in nonlinear dynamics*, Int. J. Non-Linear Mechanics 39, pp. 311-329, 2004.

3.Broer, H.W., Hoveijn, I., Lunter, G.A. and Vegter, G. *Resonances in a spring-pendulum: Algorithms for equivariant singularity theory*, Nonlinearity 11, pp. 1569-1605, 1998.

4.Cicogna, G. Gaeta,G., *Symmetry and Perturbation Theory in Nonlinear Dynamics*, Lecture Notes in Physics, Springer-Verlag, 1999.
5.Haller, G., *Chaos Near Resonance*, Applied Mathematical Sciences 138, Springer-Verlag, 1999.
6.Hénon, M. and Heiles, C., *The applicability of the third integral of motion; some numerical experiments*, Astron. J. 69, 73 (1964).
7.Holmes, P., Marsden, J. and Scheurle, J. *Exponentially small splittings of separatrices with application to KAM theory and degenerate bifurcations*, Contemp. Math. 81, pp. 213-244, 1988.
8.Hoveijn, I. and Verhulst, F. *Chaos in the* $1:2:3$ *Hamiltonian normal form*, Physica D 44, pp. 397-406, 1990.
9.Hoveijn, I. *Symplectic reversible maps, tiles and chaos*, Chaos, Solitons and Fractals 2, pp. 81-90, 1992.
10.Kozlov, V.V., *Symmetries, Topology, and Resonances in Hamiltonian Mechanics*, Ergebnisse der Mathematik und ihre Grenzgebiete 31, Springer-Verlag, 1996.
11.Kuznetsov, Yu.A., *Elements of applied bifurcation theory*, Applied Mathematical Sciences vol. 42, 3d ed., Springer-Verlag, 2004.
12.Rink, B., *Symmetry and resonance in periodic FPU chains*, Comm. Math. Phys. 218, pp. 665-685, 2001.
13.Sanders, Jan A., Verhulst, Ferdinand, Murdock, James, *Averaging methods in nonlinear dynamical systems*, Applied Mathematical Sciences vol. 59, 2d ed., Springer, 2007.
14.Verhulst, F., *Symmetry and Integrability in Hamiltonian Normal Forms*, in *Symmetry and Perturbation Theory*, D. Bambusi and G. Gaeta (eds), Quaderni GNFM pp. 245-284, Firenze, 1998.
15.Verhulst, F. and Hoveijn, I., *Integrability and chaos in Hamiltonian normal forms*, in Geometry and Analysis in Nonlinear Dynamics (H.W. Broer and F. takens, eds.), Pitman Res. Notes 222 pp. 114-134, Longman, 1992.
16.Verhulst, F., *Invariant manifolds in dissipative dynamical systems*, Acta Applicandae Mathematicae 87 pp. 229-244, 2005.
17.Verhulst, Ferdinand, *Henri Poincaré, impatient genius*, Springer, 2012.
18.Weinstein, A., *Normal modes for nonlinear Hamiltonian systems*, Inv. Math., 20, pp. 47-57, 1973.

Chaotic Modeling and Simulation (CMSIM) 1: 17–27, 2011

Stability of Solutions to Some Evolution Problems

Alexander G. Ramm

Kansas State University, Manhattan, KS 66506-2602, USA
(E-mail: ramm@math.ksu.edu)

Abstract. Large time behavior of solutions to abstract differential equations is studied. The corresponding evolution problem is:

$$\dot{u} = A(t)u + F(t,u) + b(t), \quad t \geq 0; \quad u(0) = u_0. \qquad (*)$$

Here $\dot{u} := \frac{du}{dt}$, $u = u(t) \in H$, H is a Hilbert space, $t \in \mathbb{R}_+ := [0, \infty)$, $A(t)$ is a linear dissipative operator: $\mathrm{Re}(A(t)u, u) \leq -\gamma(t)(u, u)$, $\gamma(t) \geq 0$, $F(t, u)$ is a nonlinear operator, $\|F(t, u)\| \leq c_0\|u\|^p$, $p > 1$, c_0, p are constants, $\|b(t)\| \leq \beta(t)$, $\beta(t) \geq 0$ is a continuous function.

Sufficient conditions are given for the solution $u(t)$ to problem (*) to exist for all $t \geq 0$, to be bounded uniformly on $\mathbb{R}_+$, and a bound on $\|u(t)\|$ is given. This bound implies the relation $\lim_{t\to\infty} \|u(t)\| = 0$ under suitable conditions on $\gamma(t)$ and $\beta(t)$.

The basic technical tool in this work is the following nonlinear inequality:

$$\dot{g}(t) \leq -\gamma(t)g(t) + \alpha(t, g(t)) + \beta(t),\ t \geq 0; \quad g(0) = g_0,$$

which holds on any interval $[0, T)$ on which $g(t) \geq 0$ exists and has bounded derivative from the right, $\dot{g}(t) := \lim_{s\to+0} \frac{g(t+s)-g(t)}{s}$. It is assumed that $\gamma(t)$, and $\beta(t)$ are real-valued, continuous functions of t, defined on $\mathbb{R}_+ := [0, \infty)$, the function $\alpha(t, g)$ is defined for all $t \in \mathbb{R}_+$, locally Lipschitz with respect to g uniformly with respect to t on any compact subsets $[0, T]$, $T < \infty$.If there exists a function $\mu(t) > 0$, $\mu(t) \in C^1(\mathbb{R}_+)$, such that

$$\alpha\left(t, \frac{1}{\mu(t)}\right) + \beta(t) \leq \frac{1}{\mu(t)}\left(\gamma(t) - \frac{\dot{\mu}(t)}{\mu(t)}\right), \quad \forall t \geq 0; \quad \mu(0)g(0) \leq 1,$$

then $g(t)$ exists on all of $\mathbb{R}_+$, that is $T = \infty$, and the following estimate holds:

$$0 \leq g(t) \leq \frac{1}{\mu(t)}, \quad \forall t \geq 0.$$

Keywords: Dissipative dynamical systems; Lyapunov stability; evolution problems; nonlinear inequality; differential equations..

Received: 20 September 2011 / Accepted: 21 October 2011

ISSN 2241-0503

1 Introduction

Consider an abstract nonlinear evolution problem

$$\dot{u} = A(t)u + F(t,u) + b(t), \qquad \dot{u} := \frac{du}{dt}, \tag{1}$$

$$u(0) = u_0, \tag{2}$$

where $u(t)$ is a function with values in a Hilbert space H, $A(t)$ is a linear bounded dissipative operator in H, which satisfies inequality

$$\mathrm{Re}(A(t)u,u) \leq -\gamma(t)\|u\|^2, \qquad t \geq 0; \qquad \forall u \in H, \tag{3}$$

where $F(t,u)$ is a nonlinear map in H,

$$\|F(t,u)\| \leq c_0\|u(t)\|^p, \qquad p > 1, \tag{4}$$

$$\|b(t)\| \leq \beta(t), \tag{5}$$

$\gamma(t) > 0$ and $\beta(t) \geq 0$ are continuous function, defined on all of $\mathbb{R}_+ := [0,\infty)$, $c_0 > 0$ and $p > 1$ are constants.

Recall that a linear operator A in a Hilbert space is called dissipative if $\mathrm{Re}(Au,u) \leq 0$ for all $u \in D(A)$, where $D(A)$ is the domain of definition of A. Dissipative operators are important because they describe systems in which energy is dissipating, for example, due to friction or other physical reasons. Passive nonlinear networks can be described by equation (1) with a dissipative linear operator $A(t)$, see [14], [15], Chapter 3, and [16].

Let $\sigma := \sigma(A(t))$ denote the spectrum of the linear operator $A(t)$, $\Pi := \{z : Rez < 0\}$, $\ell := \{z : Rez = 0\}$, and $\rho(\sigma,\ell)$ denote the distance between sets σ and ℓ. We assume that

$$\sigma \subset \Pi, \tag{6}$$

but we allow $\lim_{t\to\infty} \rho(\sigma,\ell) = 0$. This is the basic *novel* point in our theory. The usual assumption in stability theory (see, e.g., [1]) is $\sup_{z\in\sigma} Rez \leq -\gamma_0$, where $\gamma_0 = const > 0$. For example, if $A(t) = A^*(t)$, where A^* is the adjoint operator, and if the spectrum of $A(t)$ consists of eigenvalues $\lambda_j(t)$, $0 \geq \lambda_j(t) \geq \lambda_{j+1}(t)$, then, we allow $\lim_{t\to\infty} \lambda_1(t) = 0$. This is in contrast with the usual theory, where the assumption is $\lambda_1(t) \leq -\gamma_0$, $\gamma_0 > 0$ is a constant, is used.

Moreover, our results cover the case, apparently not considered earlier in the literature, when $\mathrm{Re}(A(t)u,u) \leq \gamma(t)$ with $\gamma(t) > 0$, $\lim_{t\to\infty} \gamma(t) = 0$. This means that the spectrum of $A(t)$ may be located in the half-plane $\mathrm{Re}z \leq \gamma(t)$, where $\gamma(t) > 0$, but $\lim_{t\to\infty} \gamma(t) = 0$.

Our goal is to give sufficient conditions for the existence and uniqueness of the solution to problem (1)-(2) for all $t \geq 0$, that is, for global existence of $u(t)$, for boundedness of $\sup_{t\geq 0} \|u(t)\| < \infty$, or to the relation $\lim_{t\to\infty} \|u(t)\| = 0$.

If $b(t) = 0$ in (1), then $u(t) = 0$ solves equation (1) and $u(0) = 0$. This equation is called zero solution to (1) with $b(t) = 0$.

Recall that the zero solution to equation (1) with $b(t) = 0$ is called Lyapunov stable if for any $\epsilon > 0$, however small, one can find a $\delta = \delta(\epsilon) > 0$, such that if $\|u_0\| \le \delta$, then the solution to Cauchy problem (1)-(2) satisfies the estimate $\sup_{t\ge 0}\|u(t)\| \le \epsilon$. If, in addition, $\lim_{t\to\infty}\|u(t)\| = 0$, then the zero solution to equation (6) is called asymptotically stable in the Lyapunov sense.

If $b(t) \not\equiv 0$, then one says that (1)-(2) is the problem with persistently acting perturbations. The zero solution is called Lyapunov stable for problem (1)-(2) with persistently acting perturbations if for any $\epsilon > 0$, however small, one can find a $\delta = \delta(\epsilon) > 0$, such that if $\|u_0\| \le \delta$, and $\sup_{t\ge 0}\|b(t)\| \le \delta$, then the solution to Cauchy problem (1)-(2) satisfies the estimate $\sup_{t\ge 0}\|u(t)\| \le \epsilon$.

The approach, developed in this work, consists of reducing the stability problems to some nonlinear differential inequality and estimating the solutions to this inequality.

In Section 2 the formulation and a proof of two theorems, containing the result concerning this inequality and its discrete analog, are given. In Section 3 some results concerning Lyapunov stability of zero solution to equation (1) are obtained. In Section 4 we derive stability results in the case when $\gamma(t) > 0$. This means that the linear operator $A(t)$ in (1) may have spectrum in the half-plane Re$z > 0$.

The results of this paper are based on the works [6]- [15]. They are closely related to the Dynamical Systems Method (DSM), see [10], [7], [8], [11].

In the theory of chaos one of the reasons for the chaotic behavior of a solution to an evolution problem to appear is the lack of stability of solutions to this problem ([2], [3]). The results presented in Section 3 can be considered as sufficient conditions for chaotic behavior not to appear in the evolution system described by problem (1)-(2).

2 Differential inequality

In this Section a self-contained proof is given of an estimate for solutions of a nonlinear inequality

$$\dot g(t) \le -\gamma(t)g(t) + \alpha(t, g(t)) + \beta(t),\ t \ge 0;\ g(0) = g_0; \quad \dot g := \frac{dg}{dt}. \tag{7}$$

In Section 3 some of the many possible applications of this estimate (estimate (11)) are demonstrated.

It is not assumed a priori that solutions $g(t)$ to inequality (7) are defined on all of $\mathbb{R}_+$, that is, that these solutions exist globally. In Theorem 1 we give sufficient conditions for the global existence of $g(t)$. Moreover, under these conditions a bound on $g(t)$ is given, see estimate (11) in Theorem 1. This bound yields the relation $\lim_{t\to\infty} g(t) = 0$ if $\lim_{t\to\infty}\mu(t) = \infty$ in (11).

Let us formulate our assumptions.

Assumption A_1). We assume that the function $g(t) \ge 0$ is defined on some interval $[0, T)$, has a bounded derivative $\dot g(t) := \lim_{s\to +0} \frac{g(t+s)-g(t)}{s}$ from the right at any point of this interval, and $g(t)$ satisfies inequality (7) at all t at which $g(t)$ is defined. The functions $\gamma(t)$, and $\beta(t)$, are real-valued, defined on all of $\mathbb{R}_+$ and continuous there. The function $\alpha(t, g) \ge 0$ is continuous on $\mathbb{R}_+ \times \mathbb{R}_+$ and locally Lipschitz with respect to g. This means that

$$|\alpha(t, g) - \alpha(t, h)| \le L(T, M)|g - h|, \tag{8}$$

if $t \in [0,T]$, $|g| \le M$ and $|h| \le M$, $M = const > 0$, where $L(T,M) > 0$ is a constant independent of g, h, and t.
Assumption A_2). There exists a $C^1(\mathbb{R}_+)$ function $\mu(t) > 0$, such that

$$\alpha\left(t, \frac{1}{\mu(t)}\right) + \beta(t) \le \frac{1}{\mu(t)}\left(\gamma(t) - \frac{\dot{\mu}(t)}{\mu(t)}\right), \quad \forall t \ge 0, \tag{9}$$

and

$$\mu(0)g(0) \le 1. \tag{10}$$

Theorem 1. *If Assumptions A_1) and A_2) hold, then any solution $g(t) \ge 0$ to inequality* (7) *exists on all of $\mathbb{R}_+$, i.e., $T = \infty$, and satisfies the following estimate:*

$$0 \le g(t) \le \frac{1}{\mu(t)} \quad \forall t \in \mathbb{R}_+. \tag{11}$$

Remark 1. *If* $\lim_{t\to\infty} \mu(t) = \infty$, *then* $\lim_{t\to\infty} g(t) = 0$.

Proof of Theorem 1. Let us rewrite inequality for μ

$$-\gamma(t)\mu^{-1}(t) + \alpha(t, \mu^{-1}(t)) + \beta(t) \le \frac{d\mu^{-1}(t)}{dt}. \tag{12}$$

Let $\phi(t)$ solve the following Cauchy problem:

$$\dot{\phi}(t) = -\gamma(t)\phi(t) + \alpha(t, \phi(t)) + \beta(t), \quad t \ge 0, \quad \phi(0) = \phi_0. \tag{13}$$

The assumption that $\alpha(t,g)$ is locally Lipschitz guarantees local existence and uniqueness of the solution $\phi(t)$ to problem (13). From the known comparison result (see, e.g., [4], Theorem III.4.1) it follows that

$$\phi(t) \le \mu^{-1}(t) \qquad \forall t \ge 0, \tag{14}$$

provided that $\phi(0) \le \mu^{-1}(0)$, where $\phi(t)$ is the unique solution to problem (14). Let us take $\phi(0) = g(0)$. Then $\phi(0) \le \mu^{-1}(0)$ by the assumption, and an inequality, similar to (14), implies that

$$g(t) \le \phi(t) \qquad t \in [0,T). \tag{15}$$

Inequalities $\phi(0) \le \mu^{-1}(0)$, (14), and (15) imply

$$g(t) \le \phi(t) \le \mu^{-1}(t), \qquad t \in [0,T). \tag{16}$$

By the assumption, the function $\mu(t)$ is defined for all $t \ge 0$ and is bounded on any compact subinterval of the set $[0,\infty)$. Consequently, the functions $\phi(t)$ and $g(t) \ge 0$ are defined for all $t \ge 0$, and estimate (11) is established.

Theorem 1 is proved. □

Let us formulate and prove a discrete version of Theorem 1.

Theorem 2. *Assume that $g_n \ge 0$, $\alpha(n, g_n) \ge 0$,*

$$g_{n+1} \le (1 - h_n\gamma_n)g_n + h_n\alpha(n, g_n) + h_n\beta_n; \quad h_n > 0, \quad 0 < h_n\gamma_n < 1, \tag{17}$$

and $\alpha(n,g_n)\geq\alpha(n,p_n)$ *if* $g_n\geq p_n$*. If there exists a sequence* $\mu_n>0$ *such that*

$$\alpha(n,\frac{1}{\mu_n})+\beta_n\leq\frac{1}{\mu_n}(\gamma_n-\frac{\mu_{n+1}-\mu_n}{h_n\mu_n}), \tag{18}$$

and

$$g_0\leq\frac{1}{\mu_0}, \tag{19}$$

then

$$0\leq g_n\leq\frac{1}{\mu_n}, \qquad \forall n\geq 0. \tag{20}$$

Proof. For $n=0$ inequality (20) holds because of (19). Assume that it holds for all $n\leq m$ and let us check that then it holds for $n=m+1$. If this is done, Theorem 2 is proved.

Using the inductive assumption, one gets:

$$g_{m+1}\leq(1-h_m\gamma_m)\frac{1}{\mu_m}+h_m\alpha(m,\frac{1}{\mu_m})+h_m\beta_m.$$

This and inequality (18) imply:

$$\begin{aligned}g_{m+1}&\leq(1-h_m\gamma_m)\frac{1}{\mu_m}+h_m\frac{1}{\mu_m}(\gamma_m-\frac{\mu_{m+1}-\mu_m}{h_m\mu_m})\\&=\mu_m^{-1}-\frac{\mu_{m+1}-\mu_m}{\mu_m^2}\leq\mu_{m+1}^{-1}.\end{aligned}$$

The last inequality is obvious since it can be written as

$$-(\mu_m-\mu_{m+1})^2\leq 0.$$

Theorem 2 is proved.

Theorem 2 was formulated in [5] and proved in [6]. We included for completeness a proof, which is shorter than the one in [6].

3 Stability results 1

In this Section we develop a method for a study of stability of solutions to the evolution problems described by the Cauchy problem (1)-(2) for abstract differential equations with a dissipative bounded linear operator $A(t)$ and a nonlinearity $F(t,u)$ satisfying inequality (4). Condition (4) means that for sufficiently small $\|u(t)\|$ the nonlinearity is of the higher order of smallness than $\|u(t)\|$. We also study the large time behavior of the solution to problem (1)-(2) with persistently acting perturbations $b(t)$.

In this paper we assume that $A(t)$ is a bounded linear dissipative operator, but our methods are valid also for unbounded linear dissipative operators $A(t)$, for which one can prove global existence of the solution to problem (1)-(2). We do not go into further detail in this paper.

Let us formulate the first stability result.

Theorem 3. *Assume that* $Re(Au,u) \leq -k\|u\|^2$ $\forall u \in H$, $k = const > 0$, *and inequality* (3) *holds with* $\gamma(t) = k$. *Then the solution to problem* (1)-(2) *with* $b(t) = 0$ *satisfies an esimate* $\|u(t)\| = O(e^{-(k-\epsilon)t})$ *as* $t \to \infty$. *Here* $0 < \epsilon < k$ *can be chosen arbitrarily small if* $\|u_0\|$ *is sufficiently small.*

This theorem implies asymptotic stability in the sense of Lyapunov of the zero solution to equation (1) with $b(t) = 0$. Our proof of Theorem 3 is new and very short.

Proof of Theorem 3. Multiply equation (1) (in which $b(t) = 0$ is assumed) by u, denote $g = g(t) := \|u(t)\|$, take the real part, and use assumption (3) with $\gamma(t) = k > 0$, to get

$$g\dot{g} \leq -kg^2 + c_0 g^{p+1}, \qquad p > 1. \tag{21}$$

If $g(t) > 0$ then the derivative $\dot{g}$ does exist, and

$$\dot{g}(t) = Re\left(\dot{u}(t), \frac{u(t)}{\|u(t)\|}\right),$$

as one can check. If $g(t) = 0$ on an open subset of $\mathbb{R}_+$, then the derivative $\dot{g}$ does exist on this subset and $\dot{g}(t) = 0$ on this subset. If $g(t) = 0$ but in in any neighborhood $(t-\delta, t+\delta)$ there are points at which g does not vanish, then by $\dot{g}$ we understand the derivative from the right, that is,

$$\dot{g}(t) := \lim_{s \to +0} \frac{g(t+s) - g(t)}{s} = \lim_{s \to +0} \frac{g(t+s)}{s}.$$

This limit does exist and is equal to $\|\dot{u}(t)\|$. Indeed, the function $u(t)$ is continuously differentiable, so

$$\lim_{s \to +0} \frac{\|u(t+s)\|}{s} = \lim_{s \to +0} \frac{\|s\dot{u}(t) + o(s)\|}{s} = \|\dot{u}(t)\|.$$

The assumption about the existence of the bounded derivative $\dot{g}(t)$ from the right in Theorem 3 was made because the function $\|u(t)\|$ does not have, in general, the derivative in the usual sense at the points t at which $\|u(t)\| = 0$, no matter how smooth the function $u(t)$ is at the point τ. Indeed,

$$\lim_{s \to -0} \frac{\|u(t+s)\|}{s} = \lim_{s \to -0} \frac{\|s\dot{u}(t) + o(s)\|}{s} = -\|\dot{u}(t)\|,$$

because $\lim_{s \to -0} \frac{|s|}{s} = -1$. Consequently, the right and left derivatives of $\|u(t)\|$ at the point t at which $\|u(t)\| = 0$ do exist, but are different. Therefore, the derivative of $\|u(t)\|$ at the point t at which $\|u(t)\| = 0$ does not exist in the usual sense.

However, as we have proved above, the derivative $\dot{g}(t)$ from the right does exist always, provided that $u(t)$ is continuously differentiable at the point t.

Since $g \geq 0$, inequality (21) yields inequality (7) with $\gamma(t) = k > 0$, $\beta(t) = 0$, and $\alpha(t,g) = c_0 g^p$, $p > 1$. Inequality (9) takes the form

$$\frac{c_0}{\mu^p(t)} \leq \frac{1}{\mu(t)}\left(k - \frac{\dot{\mu}(t)}{\mu(t)}\right), \qquad \forall t \geq 0. \tag{22}$$

Let

$$\mu(t) = \lambda e^{bt}, \qquad \lambda, b = const > 0. \tag{23}$$

We choose the constants λ and b later. Inequality (9), with μ defined in (23), takes the form

$$\frac{c_0}{\lambda^{p-1} e^{(p-1)bt}} + b \le k, \qquad \forall t \ge 0. \tag{24}$$

This inequality holds if it holds at $t = 0$, that is, if

$$\frac{c_0}{\lambda^{p-1}} + b \le k. \tag{25}$$

Let $\epsilon > 0$ be arbitrary small number. Choose $b = k - \epsilon > 0$. Then (25) holds if

$$\lambda \ge \left(\frac{c_0}{\epsilon}\right)^{\frac{1}{p-1}}. \tag{26}$$

Condition (10) holds if

$$\|u_0\| = g(0) \le \frac{1}{\lambda}. \tag{27}$$

We choose λ and b so that inequalities (26) and (27) hold. This is always possible if $b < k$ and $\|u_0\|$ is sufficiently small.

By Theorem 1, if inequalities (25)-(27) hold, then one gets estimate (11):

$$0 \le g(t) = \|u(t)\| \le \frac{e^{-(k-\epsilon)t}}{\lambda}, \qquad \forall t \ge 0. \tag{28}$$

Theorem 3 is proved. □

Remark 3. *One can formulate the result differently. Namely, choose* $\lambda = \|u_0\|^{-1}$. *Then inequality* (27) *holds, and becomes an equality. Substitute this* λ *into* (25) *and get*

$$c_0 \|u_0\|^{p-1} + b \le k.$$

Since the choice of the constant $b > 0$ *is at our disposal, this inequality can always be satisfied if* $c_0\|u_0\|^{p-1} < k$. *Therefore, condition*

$$c_0 \|u_0\|^{p-1} < k$$

is a sufficient condition for the estimate

$$\|u(t)\| \le \|u_0\| e^{-(k - c_0\|u_0\|^{p-1})t},$$

to hold (assuming that $c_0\|u_0\|^{p-1} < k$*).*

Let us formulate the second stability result.

Theorem 4. *Assume that inequalities* (3)-(5) *hold and*

$$\gamma(t) = \frac{c_1}{(1+t)^{q_1}}, \quad q_1 \le 1; \quad c_1, q_1 = const > 0. \tag{29}$$

Suppose that $\epsilon \in (0, c_1)$ *is an arbitrary small fixed number,*

$$\lambda \ge \left(\frac{c_0}{\epsilon}\right)^{1/(p-1)} \quad \textit{and} \quad \|u(0)\| \le \frac{1}{\lambda}.$$

Then the unique solution to (1)-(2) *with* $b(t) = 0$ *exists on all of* $\mathbb{R}_+$ *and*

$$0 \le \|u(t)\| \le \frac{1}{\lambda(1+t)^{c_1-\epsilon}}, \qquad \forall t \ge 0. \tag{30}$$

Theorem 4 gives the size of the initial data, namely, $\|u(0)\| \le \frac{1}{\lambda}$, for which estimate (30) holds. For a fixed nonlinearity $F(t,u)$, that is, for a fixed constant c_0 from assumption (4), the maximal size of $\|u(0)\|$ is determined by the minimal size of λ.

The minimal size of λ is determined by the inequality $\lambda \ge \left(\frac{c_0}{\epsilon}\right)^{1/(p-1)}$, that is, by the maximal size of $\epsilon \in (0, c_1)$. If $\epsilon < c_1$ and $c_1 - \epsilon$ is very small, then $\lambda > \lambda_{min} := \left(\frac{c_0}{c_1}\right)^{1/(p-1)}$ and λ can be chosen very close to λ_{min}.

Proof of Theorem 4. Let

$$\mu(t) = \lambda(1+t)^{\nu}, \qquad \lambda, \nu = const > 0. \tag{31}$$

We will choose the constants λ and ν later. Inequality (9) (with $\beta(t) = 0$) holds if

$$\frac{c_0}{\lambda^{p-1}(1+t)^{(p-1)\nu}} + \frac{\nu}{1+t} \le \frac{c_1}{(1+t)^{q_1}}, \qquad \forall t \ge 0. \tag{32}$$

If

$$q_1 \le 1 \qquad and \qquad (p-1)\nu \ge q_1, \tag{33}$$

then inequality (32) holds if

$$\frac{c_0}{\lambda^{p-1}} + \nu \le c_1. \tag{34}$$

Let $\epsilon > 0$ be an arbitrary small number. Choose

$$\nu = c_1 - \epsilon. \tag{35}$$

Then inequality (34) holds if inequality (26) holds. Inequality (10) holds because we have assumed in Theorem 4 that $\|u(0)\| \le \frac{1}{\lambda}$. Combining inequalities (26), (27) and (11), one obtains the desired estimate:

$$0 \le \|u(t)\| = g(t) \le \frac{1}{\lambda(1+t)^{c_1-\epsilon}}, \qquad \forall t \ge 0. \tag{36}$$

Condition (26) holds for any fixed small $\epsilon > 0$ if λ is sufficiently large. Condition (27) holds for any fixed large λ if $\|u_0\|$ is sufficiently small.

Theorem 4 is proved. □

Let us formulate a stability result in which we assume that $b(t) \not\equiv 0$. The function $b(t)$ has physical meaning of persistently acting perturbations.

Theorem 5. *Let* $b(t) \not\equiv 0$*, conditions* (3)- (5) *and* (29) *hold, and*

$$\beta(t) \le \frac{c_2}{(1+t)^{q_2}}, \tag{37}$$

where $c_2 > 0$ *and* $q_2 > 0$ *are constants. Assume that*

$$q_1 \le \min\{1, q_2 - \nu, \nu(p-1)\}, \qquad \|u(0)\| \le \lambda_0^{-1}, \tag{38}$$

where $\lambda_0 > 0$ *is a constant defined in* (45), *and*

$$c_2^{1-\frac{1}{p}} c_0^{\frac{1}{p}} (p-1)^{\frac{1}{p}} \frac{p}{p-1} + \nu \leq c_1. \tag{39}$$

Then problem (1)-(2) *has a unique global solution* $u(t)$, *and the following estimate holds:*

$$\|u(t)\| \leq \frac{1}{\lambda_0 (1+t)^{\nu}}, \qquad \forall t \geq 0. \tag{40}$$

Proof of Theorem 5. Let $g(t) := \|u(t)\|$. As in the proof of Theorem 4, multiply (1) by u, take the real part, use the assumptions of Theorem 5, and get the inequality:

$$\dot{g} \leq -\frac{c_1}{(1+t)^{q_1}} g + c_0 g^p + \frac{c_2}{(1+t)^{q_2}}. \tag{41}$$

Choose $\mu(t)$ by formula (31). Apply Theorem 1 to inequality (41). Condition (9) takes now the form

$$\frac{c_0}{\lambda^{p-1}(1+t)^{(p-1)\nu}} + \frac{\lambda c_2}{(1+t)^{q_2-\nu}} + \frac{\nu}{1+t} \leq \frac{c_1}{(1+t)^{q_1}} \quad \forall t \geq 0. \tag{42}$$

If assumption (38) holds, then inequality (42) holds provided that it holds for $t = 0$, that is, provided that

$$\frac{c_0}{\lambda^{p-1}} + \lambda c_2 + \nu \leq c_1. \tag{43}$$

Condition (10) holds if

$$g(0) \leq \frac{1}{\lambda}. \tag{44}$$

The function $h(\lambda) := \frac{c_0}{\lambda^{p-1}} + \lambda c_2$ attains its global minimum in the interval $[0, \infty)$ at the value

$$\lambda = \lambda_0 := \left(\frac{(p-1)c_0}{c_2} \right)^{1/p}, \tag{45}$$

and this minimum is equal to

$$h_{min} = c_0^{\frac{1}{p}} c_2^{1-\frac{1}{p}} (p-1)^{\frac{1}{p}} \frac{p}{p-1}.$$

Thus, substituting $\lambda = \lambda_0$ in formula (43), one concludes that inequality (43) holds if the following inequality holds:

$$c_0^{\frac{1}{p}} c_2^{1-\frac{1}{p}} (p-1)^{\frac{1}{p}} \frac{p}{p-1} + \nu \leq c_1, \tag{46}$$

while inequality (44) holds if

$$\|u(0)\| \leq \frac{1}{\lambda_0}. \tag{47}$$

Therefore, by Theorem 1, if conditions (46)-(47) hold, then estimate (11) yields

$$\|u(t)\| \leq \frac{1}{\lambda_0(1+t)^\nu}, \qquad \forall t \geq 0, \tag{48}$$

where λ_0 is defined in (45).

Theorem 5 is proved. □

4 Stability results 2

Let us assume that $\mathrm{Re}(A(t)u,u) \leq \gamma(t)\|u\|^2$, where $\gamma(t) > 0$. This corresponds to the case when the linear operator $A(t)$ may have spectrum in the right half-plane $\mathrm{Re} z > 0$. Our goal is to derive under this assumption sufficient conditions on $\gamma(t)$, $\alpha(t,g)$, and $\beta(t)$, under which the solution to problem (1) is bounded as $t \to \infty$, and stable. We want to demonstrate new methodology, based on Theorem 1. By this reason we restrict ourselves to a derivation of the simplest results under simplifying assumptions. However, our derivation illustrates the method applicable in many other problems.

Our assumptions in this Section are:

$$\beta(t) = 0, \quad \gamma(t) = c_1(1+t)^{-m_1}, \quad \alpha(t,g) = c_2(1+t)^{-m_2}g^p, \ p > 1.$$

Let us choose

$$\mu(t) = d + \lambda(1+t)^{-n}.$$

The constants c_j, m_j, λ, d, n, are assumed positive.

We want to show that a suitable choice of these parameters allows one to check that basic inequality (9) for μ is satisfied, and, therefore, to obtain inequality (11) for $g(t)$. This inequality allows one to derive global boundedness of the solution to (1), and the Lyapunov stability of the zero solution to (1) (with $u_0 = 0$). Note that under our assumptions $\dot\mu < 0$, $\lim_{t\to\infty}\mu(t) = d$. We choose $\lambda = d$. Then $(2d)^{-1} \leq \mu^{-1}(t) \leq d^{-1}$ for all $t \geq 0$. The basic inequality (9) takes the form

$$c_1(1+t)^{-m_1} + c_2(1+t)^{-m_2}[d+\lambda(1+t)^{-n}]^{-p+1} \leq n\lambda(1+t)^{-n-1}[d+\lambda(1+t)^{-n}]^{-1}, \tag{49}$$

and

$$g_0(d+\lambda) \leq 1. \tag{50}$$

Since we have chosen $\lambda = d$, condition (50) is satisfied if

$$d = (2g_0)^{-1}. \tag{51}$$

Choose n so that

$$n + 1 \leq \min\{m_1, m_2\}. \tag{52}$$

Then (49) holds if

$$c_1 + c_2 d^{-p+1} \leq n\lambda d^{-1}. \tag{53}$$

Inequality (53) is satisfied if c_1 and c_2 are sufficiently small. Let us formulate our result, which folows from Theorem 1.

Theorem 6. *If inequalities* (53) *and* (52) *hold, then*

$$0 \le g(t) \le [d + \lambda(1+t)^{-n}]^{-1} \le d^{-1}, \qquad \forall t \ge 0. \tag{54}$$

Estimate (54) proves global boundedness of the solution $u(t)$, and implies Lyapunov stability of the zero solution to problem (1) with $b(t) = 0$ and $u_0 = 0$.

Indeed, by the definition of Lyapunov stability of the zero solution, one should check that for an arbitrary small fixed $\epsilon > 0$ estimate $\sup_{t\ge 0} \|u(t)\| \le \epsilon$ holds provided that $\|u(0)\|$ is sufficiently small. Let $\|u(0)\| = g_0 = \delta$. Then estimate (54) yields $\sup_{t\ge 0} \|u(t)\| \le d^{-1}$, and (51) implies $\sup_{t\ge 0} \|u(t)\| \le 2\delta$. So, $\epsilon = 2\delta$, and the Lyapunov stability is proved. □

References

1.Yu. L. Daleckii and M. G. Krein, *Stability of solutions of differential equations in Banach spaces*, Amer. Math. Soc., Providence, RI, 1974.
2.B. Davies, *Exploring chaos*, Perseus Books, Reading, Massachusetts, 1999.
3.R. L. Devaney, *An introduction to chaotic dynamical systems*, Addison-Wesley, Reading, Massachusetts, 1989.
4.P. Hartman, *Ordinary differential equations*, J. Wiley, New York, 1964.
5.N.S. Hoang and A. G. Ramm, DSM of Newton-type for solving operator equations $F(u) = f$ with minimal smoothness assumptions on F, *International Journ. Comp.Sci. and Math.* (IJCSM), 3, N1/2, (2010), 3-55.
6.N. S. Hoang and A. G. Ramm, A nonlinear inequality and applications, *Nonlinear Analysis: Theory, Methods and Appl.,* 71, (2009), 2744-2752.
7.N. S. Hoang and A. G. Ramm, The Dynamical Systems Method for solving nonlinear equations with monotone operators, Asian Europ. Math. Journ., 3, N1, (2010), 57-105.
8.N. S. Hoang and A. G. Ramm, DSM of Newton-type for solving operator equations $F(u) = f$ with minimal smoothness assumptions on F, International Journ. Comp.Sci. and Math. (IJCSM), 3, N1/2, (2010), 3-55.
9.A. G. Ramm, *Dynamical systems method for solving operator equations*, Elsevier, Amsterdam, 2007.
10.A. G. Ramm, Dynamical systems method (DSM) and nonlinear problems, in the book: Spectral Theory and Nonlinear Analysis, World Scientific Publishers, Singapore, 2005, 201-228. (ed J. Lopez-Gomez).
11.A. G. Ramm, How large is the class of operator equations solvable by a DSM Newton-type method ? Appl. Math. Lett, 24, N6, (2011), 860-865.
12.A. G. Ramm, A nonlinear inequality and evolution problems, *Journ. of Inequalities and Special Functions,* 1, N1, (2010), 1-9.
13.A. G. Ramm, Asymptotic stability of solutions to abstract differential equations, *Journ. of Abstract Diff. Equations, (JADEA)*, 1, N1, (2010), 27-34.
14.A. G. Ramm, Stationary regimes in passive nonlinear networks, in the book "*Nonlinear Electromagnetics*", Editor P. Uslenghi, Acad. Press, New York, 1980, pp. 263-302.
15.A. G. Ramm, *Theory and applications of some new classes of integral equations*, Springer-Verlag, New York, 1980.
16.R. Temam, *Infinite-dimensional dynamical systems in mechanics and physics*, Springer-Verlag, New York, 1997.

Chaotic Modeling and Simulation (CMSIM) 1: 29–38, 2011

Pattern Formation of the Stationary Cahn-Hilliard Model

Hansjörg Kielhöfer

University of Augsburg, Germany
(E-mail: hansjoerg.kielhoefer@math.uni-augsburg.de)

Abstract. We investigate critical points of the free energy of the Cahn-Hilliard model of a binary alloy under the constraint of a constant mass. The domain is the unit square. Minimizers of the energy without interfacial energy term are given by a decomposition of the two components of the alloy, but the interfaces between the components are arbitrary. Specific patterns are only formed if an interfacial energy term is present. We select such patterns of minimizers by an approximation of sequences of conditionally critical points of the free energy when the interfacial energy term tends to zero. This is what we call Pattern Formation of the Stationary Cahn-Hilliard Model. Mathematically it is a singular limit process.

We obtain the conditionally critical points by a global bifurcation analysis of the Euler-Lagrange equation for the free energy where the mass is the bifurcation parameter and where the constant homogeneous mixtures give the trivial solutions. By using characteristic symmetries and monotonicities of the bifurcating solutions we show that singular limits exist for all masses in the so-called spinodal region and that they are minimizers of the free energy without interfacial energy term.

Keywords: Cahn-Hilliard model, Spinodal decomposition, Global bifurcation, Geometry of global branches, Singular limit process, Pattern formation, Weierstraß-Erdmann corner condition.

A binary alloy in a vessel Ω can be described by a function $u\colon \Omega \to \mathbb{R}$ as follows: $u(x) \in [0,1]$ means that the mixture contains $u(x) \cdot 100\,\%$ of one component at $x \in \Omega$. The energy density of the alloy is modelled by $W(u)$, where W is a two-well potential (Figure 1).

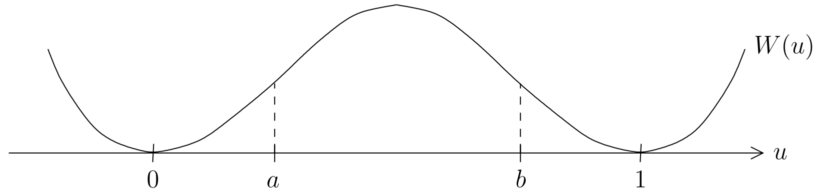

Figure 1

Received: 20 September 2011 / Accepted: 21 October 2011

ISSN 2241-0503

$W(u(x))$ is minimal, if only one component is present at $x \in \Omega$. Any mixture of the two components costs energy. The interval (a, b), where W loses its convexity, is called "spinodal region".

The total energy is given by

$$E_0(u) = \int_\Omega W(u)\,\mathrm{d}x \tag{1}$$

and the mass conservation is formulated as

$$\frac{1}{|\Omega|}\int_\Omega u\,\mathrm{d}x = m \in (0,1). \tag{2}$$

The energy (1) under the constraint (2) is minimal for the following concentrations:

$$u_0(x) = \begin{cases} 0 & \text{for } x \in \Omega_0, \\ 1 & \text{for } x \in \Omega_1, \end{cases} \tag{3}$$

with

$$\begin{aligned} |\Omega_0| &= (1-m)|\Omega|, \\ |\Omega_1| &= m|\Omega|. \end{aligned} \tag{4}$$

The following Figure 2 sketches a possible distribution of the two components in a square Ω. The decomposition of the two components is called "spinodal decomposition".

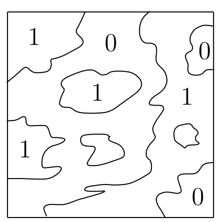

Figure 2

Only the measures of Ω_0 and Ω_1 are determined, their patterns are arbitrary. In experiments, however, certain patterns are preferred, for instance patterns with circular "interfaces".

The model is not yet complete: Taking care of the energy of the interfaces between the two components the total energy is described as

$$E_\varepsilon(u) = \int_\Omega \frac{\varepsilon}{2}\|\nabla u\|^2 + W(u)\,\mathrm{d}x, \quad \varepsilon > 0, \text{ small,} \tag{5}$$

which is called the "Cahn-Hilliard Energy".

Let u_ε be a minimizer of $E_\varepsilon(u)$ under the constraint of mass conservation. One expects for small $\varepsilon > 0$:

$$u_\varepsilon(x) \approx \begin{cases} 0 & \text{for } x \in \Omega_{0,\varepsilon}, \\ 1 & \text{for } x \in \Omega_{1,\varepsilon}, \end{cases}$$

with a profile at the interface of the form (Figure 3)

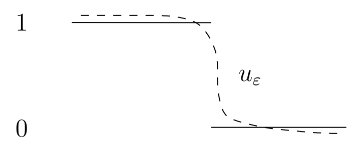

Figure 3

such that for $\varepsilon \searrow 0$

$$u_\varepsilon(x) \longrightarrow u_0(x) = \begin{cases} 0 & \text{for } x \in \Omega_{0,0}, \\ 1 & \text{for } x \in \Omega_{1,0}, \end{cases}$$

and u_0 is a minimizer of $E_0(u)$ under the same constraint.

This "singular limit process" defines the sets $\Omega_{0,0}$ and $\Omega_{1,0}$, in particular their patterns. We call it "Pattern Formation of the Stationary Cahn-Hilliard Model". Due to the "Criterion of Minimal Interface" of Modica from the year 1987, see [5], patterns with circular interfaces are created (Figure 4): If minimizers of (5) under the constraint (2) tend to u_0 in $L^1(\Omega)$ as $\varepsilon \searrow 0$, then the interface between $\Omega_{0,0}$ and $\Omega_{1,0}$ is minimal.

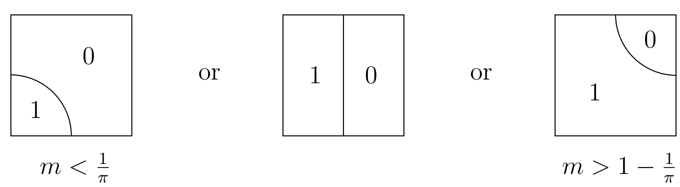

Figure 4. Criterion of Minimal Interface (Modica 1987)

For one-dimensional domains Ω this was already shown by Carr, Gurtin, and Slemrod in 1984, see [1]: The singular limit of conditional minimizers is piecewise constant with one single jump in the interval Ω.

In 1995 Grinfeld and Novick-Cohen [2] classified all conditionally critical points of (5) over an interval. They did not study their singular limits, i. e., their pattern formation.

In the sequel we study the pattern formation of conditionally critical points of (5) over the unit square Ω in $\mathbb{R}^2$. Observe that $|\Omega| = 1$. (Proofs can be found in [3], [4].)

We substitute $m = \lambda$, $u = \lambda + v$ and obtain

$$E_\varepsilon(v, \lambda) = \int_\Omega \frac{\varepsilon}{2} \|\nabla v\|^2 + W(\lambda + v)\, \mathrm{d}x \tag{6}$$

under the constraint

$$\int_\Omega v\, \mathrm{d}x = 0. \tag{7}$$

Conditionally critical points of $E_\varepsilon(v, \lambda)$ satisfy

a) the Euler-Lagrange equation:

$$-\varepsilon\Delta v + W'(\lambda + v) = \text{const.} \quad \text{in } \Omega,$$

b) the natural boundary conditions:

$$\frac{\partial v}{\partial n} = 0 \quad \text{on } \partial\Omega \text{ (Neumann boundary conditions)},$$

c) the constraint of mean value zero:

$$\int_\Omega v \,\mathrm{d}x = 0.$$

Conditions b) and c) are incorporated into a function space X and a) is expressed as

$$\begin{aligned} &G_\varepsilon(v,\lambda) := -\varepsilon\Delta v + W'(\lambda + v) - \textstyle\int_\Omega W'(\lambda+v)\,\mathrm{d}x = 0 \\ &\quad \text{for } (v,\lambda) \in X \times \mathbb{R}. \end{aligned} \tag{8}$$

We have the trivial solution

$$G_\varepsilon(0,\lambda) = 0 \quad \text{for all } \varepsilon > 0,\ \lambda \in \mathbb{R}, \tag{9}$$

which describes by $u \equiv \lambda = m$ a homogeneous mixture.

We look for nontrivial solutions (v,λ) of (8) that bifurcate from the trivial solution line $\{(0,\lambda) \mid \lambda \in \mathbb{R}\}$.

I. In the first part we fix $\varepsilon > 0$ and we consider $\lambda \in \mathbb{R}$ as a variable bifurcation parameter.

I.1 Possible bifurcation points $(0,\lambda)$ have to satisfy

$$\begin{aligned} D_v G_\varepsilon(0,\lambda)v = -\varepsilon\Delta v + W''(\lambda)v &= 0 \quad \text{in } \Omega, \\ \frac{\partial v}{\partial n} &= 0 \quad \text{on } \partial\Omega, \\ \textstyle\int_\Omega v\,\mathrm{d}x &= 0, \end{aligned} \tag{10}$$

for some nontrivial $v \in X$. This linear eigenvalue problem (10) has the solutions $v(x_1,x_2) = \cos n\pi x_1$ and $v(x_1,x_2) = \cos n\pi x_2$ for $n \in \mathbb{N}$ provided $W''(\lambda) = -\varepsilon n^2\pi^2$.

We do not consider these one-dimensional solutions here but we are rather interested in

$$\begin{aligned} v_n(x) &= \cos n\pi x_1 + \cos n\pi x_2 \quad &&\text{for } W''(\lambda) = -\varepsilon n^2\pi^2, \\ v_{nn}(x) &= \cos n\pi x_1 \, \cos n\pi x_2 \quad &&\text{for } W''(\lambda) = -2\varepsilon n^2\pi^2. \end{aligned} \tag{11}$$

The bifurcation points, which are solutions of the "characteristic equation", appear in pairs as depicted in Figure 5:

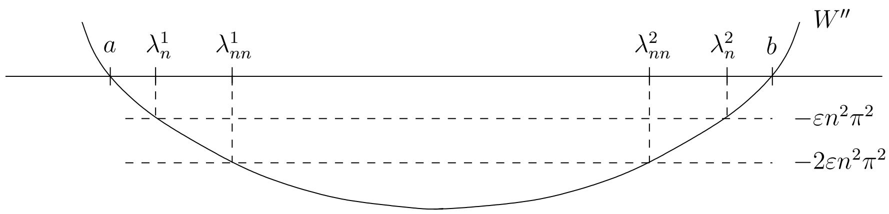

Figure 5

The number of modes $n = 1, \ldots, N(\varepsilon)$, generating bifurcation points in the spinodal region (a, b) as shown in Figure 5, tends to infinity as ε tends to zero.

The symmetries of the eigenfunctions (11) play a crucial role in the subsequent analysis. For v_n they are shown in the following Figure 6:

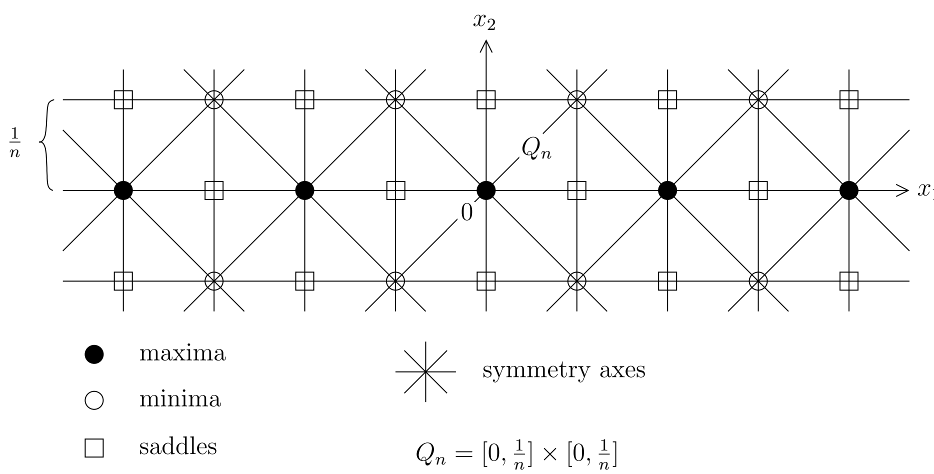

Figure 6

We define a subspace $X_n \subset X$ by the symmetries (and periodicities) of v_n and we define $X_{nn} \subset X_n \subset X$ by the symmetries (and periodicities) of v_{nn}.

I.2 We solve $G_\varepsilon(v, \lambda) = 0$ for $(v, \lambda) \in X_n \times \mathbb{R}$ as well as for $(v, \lambda) \in X_{nn} \times \mathbb{R}$. The bifurcation points are

$$(0, \lambda_{kn}^1), (0, \lambda_{kn,kn}^1), \text{and } (0, \lambda_{kn}^2), (0, \lambda_{kn,kn}^2), \quad k \in \mathbb{N}, \tag{12}$$

provided

$$W''(\lambda_{kn}^i) = -\varepsilon(kn)^2\pi^2 \quad \text{and} \quad W''(\lambda_{kn,kn}^i) = -2\varepsilon(kn)^2\pi^2 \tag{13}$$

for $i = 1, 2$. A local and global bifurcation analysis then gives the bifurcation diagram sketched in Figure 7:

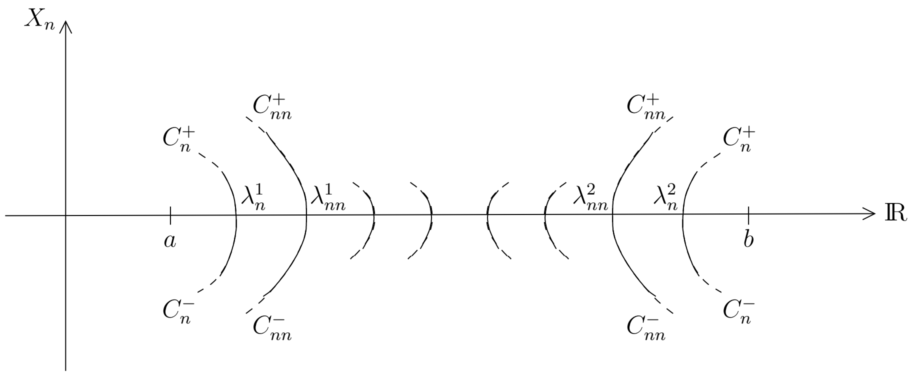

Figure 7

The branches C_n^- and C_{nn}^- are obtained from C_n^+, C_{nn}^+ by "reversion", i. e., by a reflection and a phase shift of half the period in both directions and in one direction, respectively.

By a famous result of Rabinowitz from the year 1971 all bifurcation continua are unbounded or meet the trivial solution line a second time.

I.3 In order to decide which Rabinowitz alternative holds in our case, we determine the geometry of solutions on the global continua C_n^+. (A similar analysis determines the geometry of solutions in C_{nn}^+.) We define an order in $\mathbb{R}^2$ by the positive cone $K = \{x = (x_1, x_2) \mid x_1 \geq 0, x_2 \geq 0\}$ in $\mathbb{R}^2$ (Figure 8):

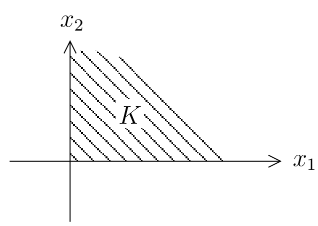

Figure 8

$$x \leq y \quad \Leftrightarrow \quad y - x \in K. \tag{14}$$

The eigenfunction v_n is monotonic in the square $Q_n = [0, \frac{1}{n}] \times [0, \frac{1}{n}]$:

$$x, y \in Q_n,\ x \leq y \quad \Rightarrow \quad v_n(x) \geq v_n(y). \tag{15}$$

By the symmetries (and periodicities) of v_n there is a monotonicity of v_n in all squares of the symmetry lattice.

By using the elliptic maximum principle and the connectivity of C_n^+ it can be shown that the monotonicity (15) is preserved for all solutions of $G_\varepsilon(v, \lambda) = 0$ on C_n^+:

$$x, y \in Q_n,\ x \leq y \quad \Rightarrow \quad v(x) \geq v(y) \tag{16}$$

The consequences of (16) are that the location of the maxima, minima, and saddles is fixed for all solutions on C_n^+. This, in turn, implies that all bifurcating continua C_n^+ and C_{nn}^+ are separated.

I.4 The geometry of solutions on C_n^+ described before helps to derive the following a priori estimates:

$$\begin{aligned} (v,\lambda) \in C_n^+ \quad \Rightarrow \quad & \|v\|_{L^\infty(\Omega)} + |\lambda| \le M_1, \\ & \|v\|_{C^{2+\alpha}(\overline{\Omega})} \le M_2/\varepsilon^2, \end{aligned} \tag{17}$$

where M_1 and M_2 do not depend on $\varepsilon > 0$. The results of I.3 and (17) then yield the global bifurcation diagram sketched in Figure 9:

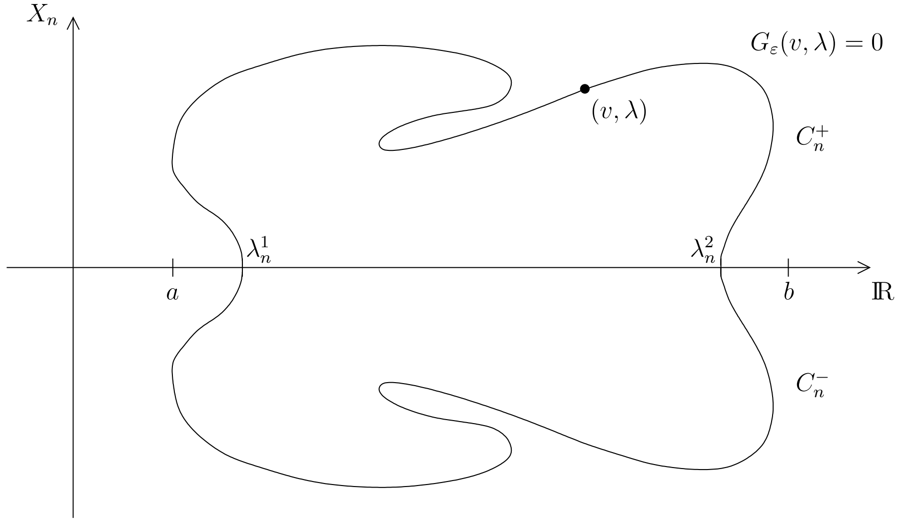

Figure 9

The turning points are explained later.

II. In the second part we fix λ in the spinodal region (a,b) and let ε tend to 0. Since the solution continua C_n^+ depend on ε we change the notation:

$$\begin{aligned} & C_n^+ = C_{n,\varepsilon}^+ \\ & (v,\lambda) \in C_{n,\varepsilon}^+ \quad \Rightarrow \quad v = v_{\lambda,\varepsilon}, \quad \text{where } G_\varepsilon(v_{\lambda,\varepsilon},\lambda) = 0. \end{aligned} \tag{18}$$

II.1 Let $\varepsilon_n \searrow 0$ and consider the sequence $(v_{\lambda,\varepsilon_n})_{n\in\mathbb{N}}$ in $L^p(\Omega)$. The estimates $\|v_{\lambda,\varepsilon_n}\|_{L^\infty(\Omega)} \le M_1$ and $\|v_{\lambda,\varepsilon_n}\|_{C^{2+\alpha}(\overline{\Omega})}\| \le M_2/\varepsilon_n^2$ do not imply that this sequence is relatively compact in $L^p(\Omega)$ for $1 \le p < \infty$. However, by the monotonicity (16) it is relatively compact in $L^p(Q_n)$, and therefore, by the symmetries (and periodicities), it is relatively compact in $L^p(\Omega)$. This follows by an extension of Helly's theorem on one-dimensional monotonic sequences to two dimensions. Thus we can state (w. l. o. g.):

$$\begin{aligned} v_{\lambda,\varepsilon_n} \longrightarrow v_{\lambda,0} \quad & \text{in } L^p(\Omega) \text{ for } 1 \le p < \infty \\ \text{as } \varepsilon_n \searrow 0. & \end{aligned} \tag{19}$$

II.2 The properties of the singular limit $v_{\lambda,0} \in L^p(\Omega)$ are:

a) $\displaystyle\int_\Omega v_{\lambda,0}\,\mathrm{d}x = 0$,

b) $v_{\lambda,0} \in X_n$, $v_{\lambda,0}$ is monotonic in Q_n,

c) $\lambda + v_{\lambda,0} = u_{\lambda,0}$ is a conditionally critical point of $E_0(u) = \int_\Omega W(u)\,\mathrm{d}x$, i. e., $W'(u_{\lambda,0}) = \text{const.}$,

d) $v_{\lambda,0} \neq 0$, i. e., $v_{\lambda,0}$ is nontrivial,

e) $u_{\lambda,0}$ has precisely two values.

Property d) is not obvious. It follows from $W''(u_{\lambda,0}) \geq 0$, which, in turn, is a consequence of the variational characterization of the positive principal eigenvalue of an eigenvalue problem with weight function. Property e) then follows from c) and $W''(u_{\lambda,0}) \geq 0$. Finally,

f) $u_{\lambda,0}$ is a global minimizer of $E_0(u)$ under the constraint $\int_\Omega u\,\mathrm{d}x = \lambda = m \in (a,b)$.

Property f) is not obvious as well. It follows from the second Weierstraß-Erdmann corner condition developed for discontinuous global minimizers of one-dimensional variational problems:

$$\begin{array}{l} W(u_{\lambda,0}) - u_{\lambda,0}W'(u_{\lambda,0}) \text{ is continuous,} \\ \text{which means constant by e).} \end{array} \tag{20}$$

Property (20) admits only the following two values for $u_{\lambda,0}$ which proves f):

$$u_{\lambda,0}(x) = \begin{cases} 0 & \text{for } x \in \Omega_{0,0}, \\ 1 & \text{for } x \in \Omega_{1,0}, \end{cases} \tag{21}$$

where the sets $\Omega_{0,0}$ and $\Omega_{1,0}$ depend on $\lambda = m$. This accomplishes the pattern formation of the stationary Cahn-Hilliard model.

For $n = 4$ we obtain the following pattern in X_n (Figure 10):

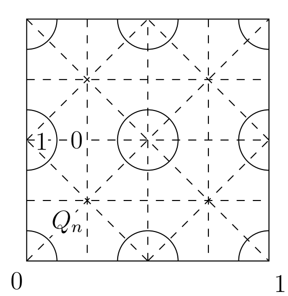

Figure 10

In the symmetry class X_{nn} a pattern for $n = 4$ is the following Figure 11:

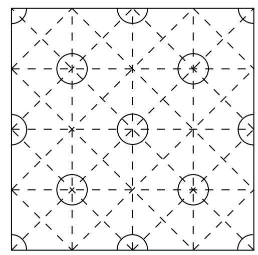

Figure 11

The interfaces are circular, if $u_{\lambda,\varepsilon}$ are conditional mimimizers of $E_\varepsilon(u)$.

However, not all $u_{\lambda,\varepsilon} = \lambda + v_{\lambda,\varepsilon}$, where $(v_{\lambda,\varepsilon}, \lambda) \in C^+_{n,\varepsilon}$, are minimizers with mean value $\lambda = m \in (a, b)$.

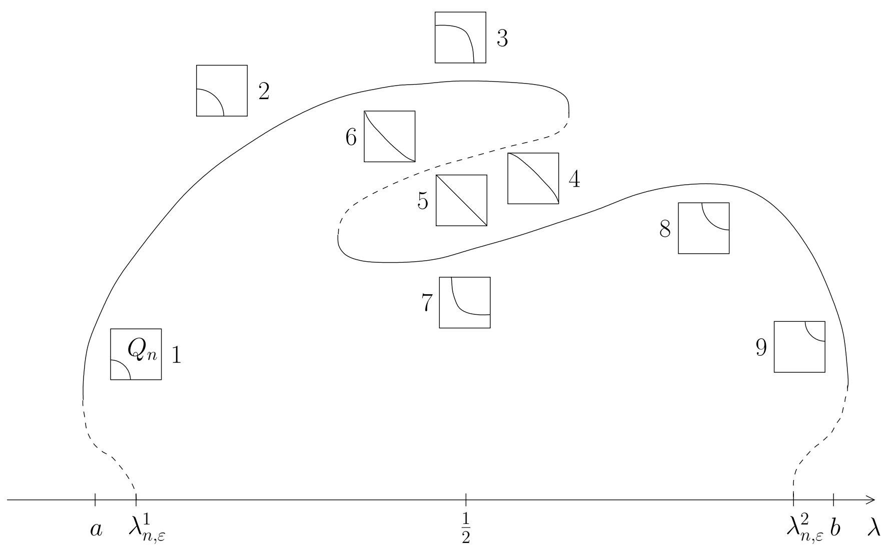

Figure 12

Figure 12 sketches the global continuum $C^+_{n,\varepsilon}$ for small $\varepsilon > 0$. A continuous transition from pattern 1 to pattern 9 in keeping the monotonicity and symmetry of $u_{\lambda,\varepsilon}$ in Q_n is only possible through patterns 4, 5, 6, which are not created by minimizers, since the interface is not minimal. Therefore the continuum has to have two additional turning points, where the stability changes. In particular, the continuum with patterns 4, 5, 6 is unstable, i. e., the critical points $u_{\lambda,\varepsilon}$ are not minimizers. These heuristic arguments for the turning points are verified by a numerical pathfollowing.

References

1.J. Carr, M. E. Gurtin, and M. Slemrod. Structured Phase Transitions on a Finite Interval. Archive for Rational Mechanics and Analysis **86**, 317–351, 1984.

2.M. Grinfeld and A. Novick-Cohen. Counting stationary solutions of the Cahn-Hilliard equation by transversality arguments. Proceedings of the Royal Society of Edinburgh **125A**, 351–370, 1995.
3.H. Kielhöfer. Pattern Formation of the Stationary Cahn-Hilliard Model. Proceedings of the Royal Society of Edinburgh **127A**, 1219–1243, 1997.
4.H. Kielhöfer. Minimizing Sequences Selected via Singular Perturbations, and their Pattern Formation. Archive for Rational Mechanics and Analysis **155**, 261–276, 2000.
5.L. Modica. The Gradient Theory of Phase Transitions and the Minimal Interface Criterion. Archive for Rational Mechanics and Analysis **98**, 123–142, 1987.

Chaotic Modeling and Simulation (CMSIM) 1: 39–50, 2011

BetaBoop Brings in Chaos

Maria de Fátima Brilhante[1], Maria Ivette Gomes[2] and Dinis Pestana[3]

[1] Universidade dos Açores and CEAUL, Ponta Delgada, Açores, Portugal
(E-mail: fbrilhante@uac.pt)
[2] Universidade de Lisboa and CEAUL, Lisboa, Portugal
(E-mail: ivette.gomes@fc.ul.pt)
[3] Universidade de Lisboa and CEAUL, Lisboa, Portugal
(E-mail: dinis.pestana@fc.ul.pt)

Abstract. The Verhults differential equation $\frac{\mathrm{d}}{\mathrm{d}t}N(t) = r\,N(t)\,(1-N(t))$ and its logistic parabola difference equation counterpart $x_{t+1} = \alpha x_t\,(1-x_t)\,\mathrm{I}_{(0,1)}(x_t)$, $\alpha \in [0,4]$, are tied to sustainable growth. We investigate the implications of considering $1-N(t)$, the linear truncation of the MacLaurin expansion of $-\ln N(t)$, or $N(t)$, the linear truncation of $-\ln(1-N(t))$, i.e. of curbing down either the retroaction factor $1-N(t)$ or the growing factor $N(t)$, which leads to Gumbel extreme value population for maxima or minima, respectively. More generally, we consider $\frac{\mathrm{d}}{\mathrm{d}t}N(t) = r\,N(t)\,(-\ln N(t))^{1+\gamma^*}$ — or, alternatively, $\frac{\mathrm{d}}{\mathrm{d}t}N(t) = r\,(-\ln(1-N(t)))^{1+\gamma^*}\,(1-N(t))$ —- and its difference equation counterpart. Simple extensions of the beta densities arise naturally in this context, and we discuss a $BetaBoop(p,q,P,Q)$, $p,q,P,Q>0$ family of probability density functions, that for $P=Q=1$ reduces to the usual $Beta(p,q)$ family.
Keywords: Population dynamics and chaos, extremal models, beta family.

1 Introduction

The rationale of the Verhulst population dynamics model

$$\frac{\mathrm{d}}{\mathrm{d}t}N(t) = r\,N(t)\,(1-N(t)) \tag{1}$$

is well-known: due to the malthusian reproduction rate $r>0$, $r\,N(t)$ implies growth, but on the other hand the retroaction term $-r\,N^2(t)$ slows down the growth impetus, and ultimately dominates, an action that is often interpreted in terms of sustainability. Hence the logistic solution of (1), $N(t) = 1/(1+\mathrm{e}^{-rt})$ (normalized so that $N(t)$ is a probability distribution function), is often tied to the idea of sustainable population dynamics growth.

Using Euler's algorithm, with an appropriate factor s, the equation (1) can be rewritten as

$$N(t+1) = N(t) + sr\,N(t)\,(1-N(t)) \quad\Longleftrightarrow\quad x_{t+1} = \alpha x_t\,(1-x_t) \tag{2}$$

Received: 20 September 2011 / Accepted: 21 October 2011

ISSN 2241-0503

where $x_t = sr\,N(t)/(sr+1)$, $\alpha = 1+sr$; if $\alpha \in (0,4)$, $x_t \in (0,1) \Longrightarrow x_{t+1} \in (0,1)$.

Due to its connection to the logistic curve, $\alpha\, x\,(1-x)\mathrm{I}_{(0,1)}(x)$ is sometimes referred to as logistic parabola. Observe that, with the notation $X_{p,q} \frown Beta(p,q)$, $\alpha\, x\,(1-x)\,\mathrm{I}_{(0,1)}(x) = \frac{\alpha}{6}\, f_{X_{2,2}}(x)$, where $f_{X_{2,2}}(x) = 6\,x\,(1-x)\,\mathrm{I}_{(0,1)}(x)$ is the probability density function of $X_{2,2} \frown Beta(2,2)$.

The fact that Euler's algorithm transforms the logistic differential equation in the difference equation model $x_{n+1} = \alpha\, x_n\,(1-x_n)$ had an important impact in the recognition that bifurcations, fractality, and ultimate chaos were indeed important tools in modeling population dynamics, when the reproduction rate r is explosive and sustainability fails.

As the Verhulst model is closely tied to the $Beta(2,2)$ probability density function, Aleixo *et al.* [1], [2], investigated the population dynamics of its natural extensions tied to general $Beta(p,q)$ models. Explicit solutions of the differential equation $\frac{\mathrm{d}}{\mathrm{d}t}N(t) = r\,N^{p-1}(t)\,(1-N(t))^{q-1}$ exist only for some (p,q) other than $(2,2)$ — for instance, $4\,\mathrm{e}^{rt}/\,(1+\mathrm{e}^{rt})^2$ is the solution of $\frac{\mathrm{d}}{\mathrm{d}t}N(t) = r\,N(t)\,\sqrt{1-N(t)}$ — but using appropriate software (we used *Mathematica* 7) numerical approximations of the solutions of practical problems are easily worked out.

As $\ln N(t) = -\sum_{k=1}^{\infty}(1-N(t))^k/k$, the factor $1-N(t)$ in (1) may be looked at as the linear truncation of $-\ln N(t)$. In the differential equation

$$\frac{\mathrm{d}}{\mathrm{d}t}N(t) = r\,N(t)\,(-\ln N(t)), \tag{3}$$

the retroaction factor $-\ln N(t)$ is much lighter than $1-N(t)$, and hence it is not surprising that the solution of (3), $N(t) = \mathrm{e}^{-\mathrm{e}^{-rt}}$ (once again normalized to be a probability distribution function) is one of the extreme value laws for maxima, namely the Gumbel law.

On the other hand $\ln(1-N(t)) = -\sum_{k=1}^{\infty} N^k(t)/k$, and considering that the growing factor $N(t)$ in (1) is the linear approximation of $-\ln(1-N(t))$, we may regard (1) as an approximation of

$$\frac{\mathrm{d}}{\mathrm{d}t}N(t) = r\,(-\ln(1-N(t)))\,(1-N(t)) \tag{4}$$

whose solution, once again normalized, is the Gumbel extreme value distribution for minima, $N(t) = 1-\mathrm{e}^{-\mathrm{e}^{rt}}$, which makes sense since in this case we curbed down the growing factor.

Pestana *et al.* [9] investigated $\frac{\mathrm{d}}{\mathrm{d}t}N(t) = r\,N(t)\,(-\ln N(t))$ and its discretization counterpart $x_{t+1} = s\,r\,x_t(-\ln x_t)$ in modeling extremal growth rate, as observed in the dynamics of cancer cells populations.

The generalization

$$f_{p,Q}(x) = \frac{p^Q}{\Gamma(Q)}\,x^{p-1}(-\ln x)^{Q-1}\mathrm{I}_{(0,1)}(x)$$

of the beta densities, has been introduced by Brilhante *et al.* [3]. In Section 2 we discuss the behavior of $x_{t+1} = r\,x_t(-\ln x_t)\,\mathrm{I}_{(0,1)}(x)$, the more general differential equation $\frac{\mathrm{d}}{\mathrm{d}t}N(t) = r\,N(t)\,(-\ln N(t))^{1+\gamma}$ and its connection to extreme value laws, as well as the behavior of $x_{t+1} = s\,r\,x_t(-\ln x_t)^{1+\frac{1}{\gamma}}\mathrm{I}_{(0,1)}(x)$. In Section 3 we introduce a new extension of the beta densities, namely

$$f_{p,q,P,Q}(x) = c\,x^{p-1}(1-x)^{q-1}(-\ln(1-x))^{P-1}(-\ln x)^{Q-1}\mathrm{I}_{(0,1)}(x), \qquad (5)$$

$p, q, P, Q > 0$, and a general discussion on modeling population dynamics via differential equations/difference equations, questioning whether chaos is in fact an appropriate framework in the description of evolution of populations.

2 Extreme value laws and population dynamics

As observed in Section 1, the Gumbel distribution function for maxima, $N(t) = \mathrm{e}^{-\mathrm{e}^{-rt}}$, is a solution of the differential equation $\frac{\mathrm{d}}{\mathrm{d}t}N(t) = r\,N(t)\,(-\ln N(t))$, and the Gumbel distribution function for minima, $N^*(t) = 1 - \mathrm{e}^{-\mathrm{e}^{rt}}$, is a solution of the differential equation $\frac{\mathrm{d}}{\mathrm{d}t}N^*(t) = r\,(-\ln(1-N^*(t)))\,(1-N^*(t))$. We now consider difference equations closely tied to those differential equations, i.e., we assume that there exists an appropriate c such that

$$N(t+1) = N(t) + cN(t)\,(-\ln N(t)) \Longleftrightarrow N(t+1) = -c\,N(t)\,\ln\left(\frac{N(t)}{\mathrm{e}^{\frac{1}{c}}}\right),$$

and we obtain the difference equation,

$$x_{t+1} = c\,x_t\,(-\ln x_t), \qquad (6)$$

closely associated to (3). As long as $x_t \in (0,1)$, if $c \in (0, \mathrm{e})$ we also have $x_{t+1} \in (0,1)$. The stationary solutions of (6) are $x_{t+1} = x_t = x_0$ with $x_0 = 0$ or $x_0 = \mathrm{e}^{-\frac{1}{c}}$. In view of the stability criterion for the stationary solutions, $\left|c\,(-\ln x - 1)\right| < 1$, and hence the stationary solution $x_0 = \mathrm{e}^{-\frac{1}{c}}$ is stable for $0 < c < 2.$, cf. Fig. 1

Using in *Mathematica* 7 the output of the instructions

```
Clear[f, x]
f[c_][x_] := c x *(-Log[x]) // N
x[c_][n_] := x[c][n] = f[c][x[c][n - 1]] // N
x[c_][0] := 0 // N;
tb = Table[{c, x[c][n]}, {c, .1, Exp[1], .01}, {n, 1000, 1300}];
Short[tb]
```

as input for the instructions

```
tb2 = Flatten[tb, 1];
ListPlot[tb]
```

we obtain the graph in Fig. 2, exhibiting bifurcations for $c \geq 2$, and ultimately chaos, as expected from the observations above.

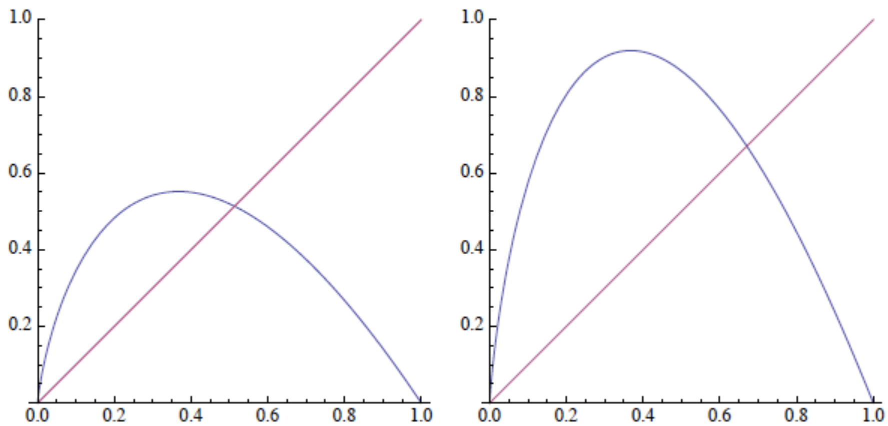

Fig. 1. Left: $1.5\, x_t\,(-\ln x_t)$; right: $2.5\, x_t\,(-\ln x_t)$.

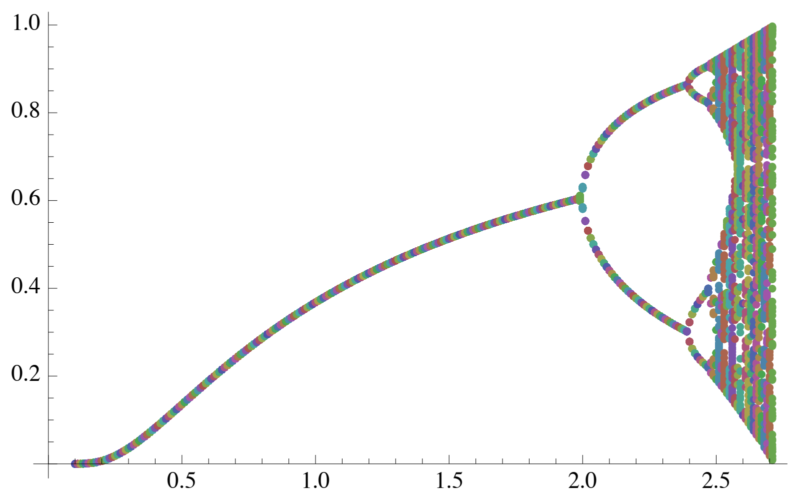

Fig. 2. Bifurcation diagram, solving $x = f(c, x) = c\, x\,(-\ln x)$, $c \in (0, \mathrm{e})$, using the fixed point method.

As we have discussed previously, the Gumbel distribution for minima $N(t) = 1 - \mathrm{e}^{-\mathrm{e}^{rt}}$ is a solution for the differential equation $\frac{\mathrm{d}}{\mathrm{d}t} N^*(t) = r\,(-\ln(1 - N^*(t)))\,(1 - N^*(t))$, which is tied to the difference equation $x_{t+1} = c(-\ln(1 - N(t)))\,(1 - N(t))$. Fig. 3 is the simile of Fig. 2 for this case.

A more general situation involves the study of the differential equations

- $\frac{\mathrm{d}}{\mathrm{d}t} N(t) = r\, N(t)\,(-\ln N(t))^{1+\frac{1}{\gamma}}$, whose solution for $\gamma > 0$ is (again in standardized form) the Fréchet distribution function for maxima $N(t) = \mathrm{e}^{-(\frac{r}{\gamma} x)^{-\gamma}}\, \mathrm{I}_{[0,\infty)}(t)$, and whose solution for $\gamma < 0$ is the Weibull distribution function for maxima $N(t) = \mathrm{e}^{-(-\frac{r}{\gamma} t)^{\gamma}}\, \mathrm{I}_{(-\infty,0)}(t) + 1\, \mathrm{I}_{[0,\infty)}(t)$.

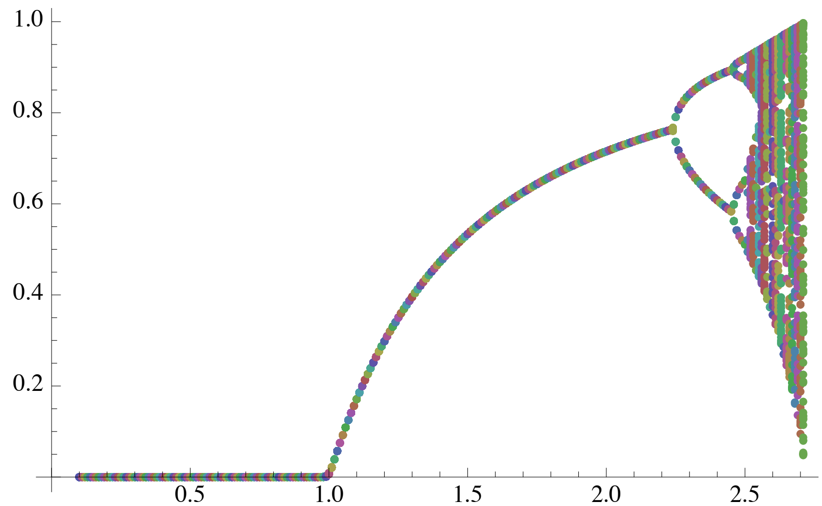

Fig. 3. Bifurcation diagram, solving $x = f(c, x) = c\,(-\ln(1-x))\,(1-x)$, $c \in (0, \mathrm{e})$, using the fixed point method.

- $\frac{\mathrm{d}}{\mathrm{d}t} N(t) = r\,N(t)\,(-\ln N(t))^{1+\frac{1}{\gamma}}$, whose solution for $\gamma > 0$ is the Fréchet distribution for minima, and for $\gamma < 0$ is the Weibull distribution function for minima.

Fig. 4 and Fig. 5 illustrate the dynamical behavior when solving by the fixed point method the difference equations closely associated to the above differential equations, namely $x_{t+1} = c\,x_t\,(-\ln x_t)^{1+\frac{1}{\gamma}}$ for $\gamma = 1$ (Fréchet-1) and $\gamma = -2$ (Weibull-0.5).

Remark 1. Considering the *G*eneral *E*xtreme *V*alue (*GEV*) distribution for maxima, $G_{\gamma^*}(t) = \mathrm{e}^{-(1+\gamma^* t)^{-1/\gamma^*}}$, $1 + \gamma^* t > 0$, it is obvious, from

$(1+\gamma^* t)^{-1/\gamma^*-1} = \left((1+\gamma^* t)^{-1/\gamma^*}\right)^{\frac{1/\gamma^*+1}{1/\gamma^*}} = (-\ln G_{\gamma^*}(t))^{1+\gamma^*}$, that G_{γ^*} satisfies the differential equation

$$\frac{\mathrm{d}}{\mathrm{d}t} G_\gamma(t) = G_\gamma(t)\,(-\ln G_\gamma(t))^{1+\frac{1}{\gamma}},\ \gamma = \frac{1}{\gamma^*}.$$

In the *GEV* representation, a shape parameter $\gamma^* > 0$ corresponds to the Fréchet-$\frac{1}{\gamma^*}$, $\gamma^* < 0$ corresponds to the Weibull-$\frac{1}{|\gamma^*|}$, and $\gamma^* \to 0$ corresponds to the Gumbel.

The similarity of

$$\frac{\mathrm{d}}{\mathrm{d}t} N(t) = r\,N(t)\,(-\ln N(t))^{1+\frac{1}{\gamma}}$$

and

$$\frac{\mathrm{d}}{\mathrm{d}t} N(t) = r\,(-\ln(1-N(t)))^{1+\frac{1}{\gamma}}\,(1-N(t))$$

comes from the fact that stable distributions G for maxima (either Gumbel, or Fréchet or Weibull) and the corresponding stable distributions G^* for minima are tied through the relationship $G^*(x) = 1 - G(-x)$.

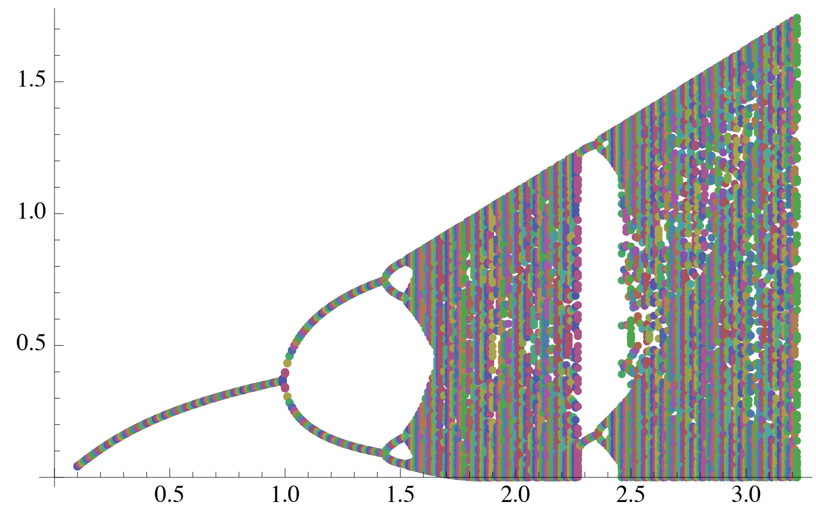

Fig. 4. Bifurcation diagram, solving $x = f(c,x) = c\,x\,(-\ln x)^2$ using the fixed point method.

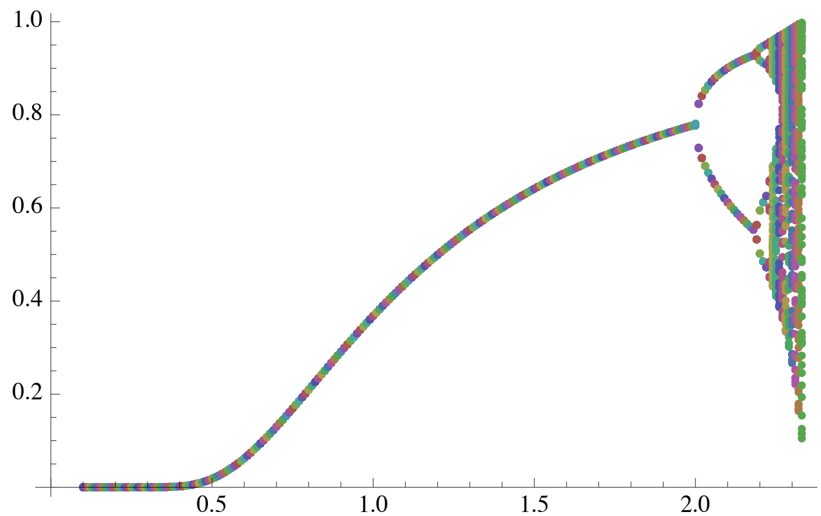

Fig. 5. Bifurcation diagram, solving $x = f(c,x) = c\,x\,(-\ln x)^{0.5}$ using the fixed point method.

3 The BetaBoop family

Brilhante *et al.* [3] extensively studied the family of probability density functions

$$f_{p,Q}(x) = \frac{p^Q}{\Gamma(Q)}\, x^{p-1}(-\ln\, x)^{Q-1}\, \mathrm{I}_{(0,1)}(x),$$

$p, Q > 0$, and their relevance in population studies.

Denote $X_{p,Q} \frown Betinha(p,Q)$, $p,Q>0$, the random variable whose probability density function is $f_{p,Q}$, given above.

In fact, $4\,x\,(-\ln x)\,\mathrm{I}_{(0,1)}(x)$, tied to the Gumbel model, is the case $p=Q=2$ in this family, just as $6\,x\,(1-x)\,\mathrm{I}_{(0,1)}(x)$, tied to the logistic parabola and the Verhulst population model, is the case $p=q=2$ of the $Beta(p,q)$ family of probability density functions, whose dynamical behavior has been studied in depth in Aleixo *et al.* [1], [2], and references therein. This new family provides difference models whose associated differential models have as solution, among others, the stable distributions for maxima.

In the previous section we have seen that the probability density function of random variables $Y_{P,q}=1-X_{q,P}$, with $q=2$, are connected to difference equations associated to differentail equations having as solutions the stable distributions for minima.

In fact, in view of Hölder's inequality, the function

$$x^{p-1}(1-x)^{q-1}(-\ln(1-x))^{P-1}(-\ln x)^{Q-1}\,\mathrm{I}_{(0,1)}(x)$$

is integrable for every $p,q,P,Q>0$, and hence there exists $c\in(0,\infty)$ such that $f_{p,q,P,Q}$, in (5), is a probability density function. We denote the corresponding random variable $X_{p,q,P,Q} \frown BetaBoop(p,q,P,Q)$. Observe that $BetaBoop(p,q,1,1)$ is the same as $Beta(p,q)$, and $BetaBoop(p,1,P,1)$ is the same as $Betinha(p,P)$.

Betty Boop brought in chaos to the American Board of Censorship — sorry, we were dreaming of Betty Boop and Jessica Rabbit, and what we really meant to say is $BetaBoop(p,q,P,Q)$ brings in chaos, in the sense that the fixed point solution of equations of the type

$$x=c\,x^{p-1}(1-x)^{q-1}(-\ln(1-x))^{P-1}(-\ln x)^{Q-1}$$

exhibit all the problems first encountered in the numerical solution of the case $p=q=2$, $P=Q=1$. In Fig. 6 we illustrate this for $p=q=P=Q=1.5$, and in Fig. 7 for $p=q=1, P=Q=3$.

In fact, many other generalizations of the logistic parabola

$f_c(x)=cx(1-x)\,\mathrm{I}_{(0,1)}(x)$ are potentially interesting in modeling population dynamics, as far as they reflect recognizable characteristics. For instance, the linear truncation of $\mathrm{e}^{-x}\approx(1-x)$ shows that $c\,x\,\mathrm{e}^{-x}\,\mathrm{I}_{(0,1)}(x)\approx c^*\,x\,(1-x)\,\mathrm{I}_{(0,1)}(x)$. In Fig. 8 we represent the bifurcation diagram corresponding to the difference equation $x_{t+1}=c\,x\,\mathrm{e}^{-x}$, modeling extremely slow growth.

Tsoularis, [10], in his overview of extensions of the logistic growth model, describes a *hyper-Gompertz* class, introduced by Turner *et al.*, [11], which is a subclass of the BetaBoop family. Our approach, using retroaction factor functions whose linearization is $(1-x)$ (such as $-\ln\,x$ or e^{-x}) and/or growing factor functions for which x is the linear truncation (such as $-\ln(1-x)$), leads to a wider class of growth models. Knowledge of the biological population dynamics may serve as an educated guess guideline to choose appropriate growth and retroaction factors, and as a basis to choose among competing growth models.

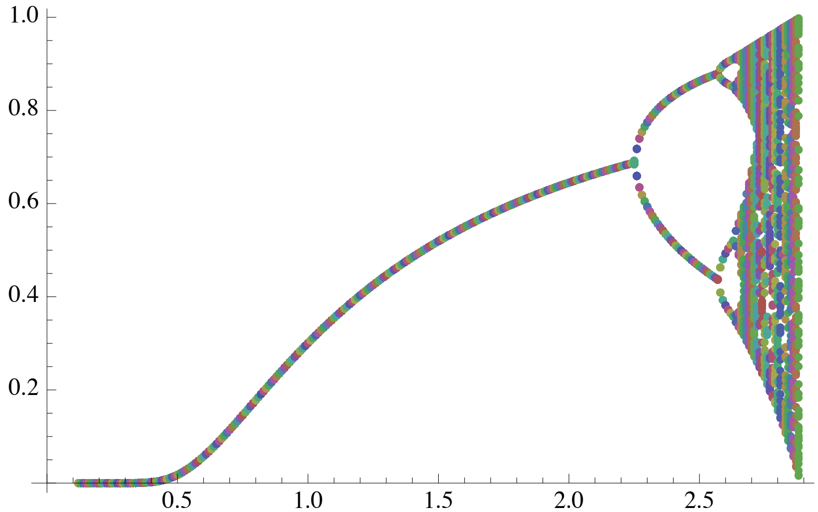

Fig. 6. Bifurcation diagram, solving $x = f(c,x) = c(x(1-x)(-\ln(1-x))(-\ln x))^{0.5}$ using the fixed point method.

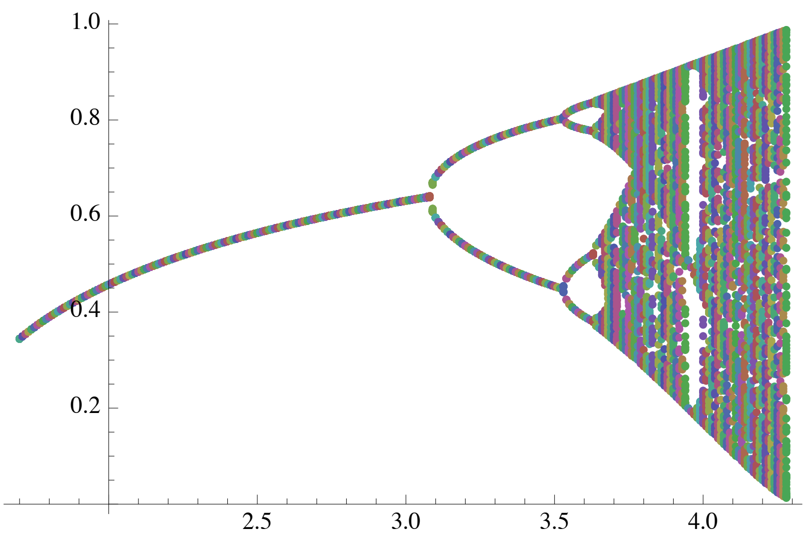

Fig. 7. Bifurcation diagram, solving $x = f(c,x) = c((-\ln x\,(-\ln(1-x)))^2$ using the fixed point method.

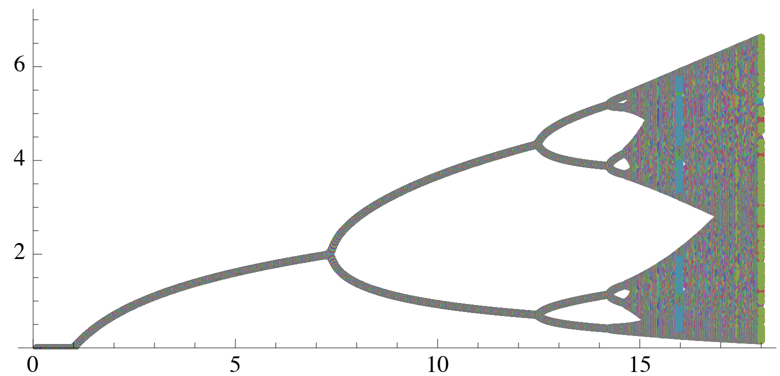

Fig. 8. Bifurcation diagram, solving $x = f(c, x) = c\,x\,\mathrm{e}^{-x}$ using the fixed point method.

4 Avoiding Chaos and a Class of New Non-Stable Extreme Value Laws

Finally, let us remark that there are grounds to argue that the chaos map $\big($for instance $x_{t+1} = c\,x_t\,(-\ln x_t)\big)$ is not an appropriate discrete equivalent of the original differential equation — for that example, $\frac{\mathrm{d}}{\mathrm{d}t}N(t) = r\,N(t)\,(-\ln N(t))$ —, inasmuch as the chaos map implies bifurcations and ultimately chaos, inexistent in the original differential equation.

An interesting point is that if we consider that the retroaction acts at time $t+1$, we obtain a difference equation $x_{t+1} = c\,x_t\,(-\ln x_{t+1})$, that has the same stationary solutions as the chaos map $x_{t+1} = c\,x_t\,(-\ln x_t)$, but does not exhibit bifurcation and chaos. In fact, from $x_{t+1} = c\,x_t\,(-\ln x_{t+1})$ we get a solution $f_c(x) = cx\,W\left(\frac{1}{cx}\right)$, where $W()$ is the Logarithmic Product function, a function taking on real values for $x > -0.5$.

Fig. 9 below shows that $cx\,W\left(\frac{1}{cx}\right)\,\mathrm{I}_{(0,\infty)}(x)$ is a distribution function, that may serve as a non-stable extreme value law, but that definitively is not a good approximation to the Gumbel distribution. (We used $c = 2$, and computed the Gumbel scale parameter 0.52688, so that the the lines cross at the 0.9 quantile.)

This is patently a rather poor approximation, even for quite large values. In fact, investigating this approximation has been motivated solely from the fact that this is a non-chaotic solution of a modified difference equation approximation to the differential equation whose solution is the Gompertz curve, i.e. the Gumbel distribution, when properly normalized.

In fact

$$\lim_{x\to\infty} \frac{1 - ctx\,W\,(1/(ctx))}{1 - cx\,W\,(1/(cx))} = t^{-1},$$

showing that this new law is in the domain of attraction of the Fréchet with shape parameter 1, whatever the value $c > 0$.

Fig. 10, comparing the distribution function $2x\,W\left(\frac{1}{2x}\right)\,\mathrm{I}_{(0,\infty)}(x)$ and the Fréchet distribution $\mathrm{e}^{-\frac{0.44995}{x}}\,\mathrm{I}_{(0,\infty)}(x)$, shows that this approximation is quite

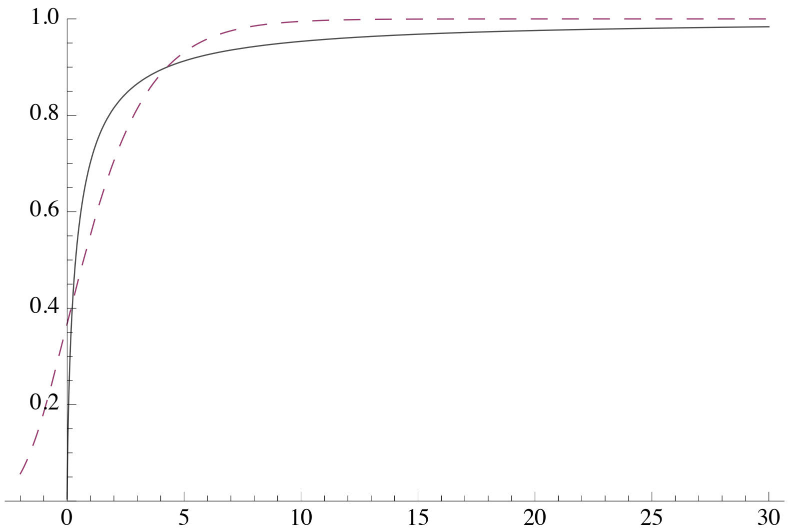

Fig. 9. $2x\,W\left(\frac{1}{2x}\right)\,\mathrm{I}_{(-0,\infty)}(x)$ (solid line) approximation of $\mathrm{e}^{-\mathrm{e}^{-0.52688\,x}}$ (dashed line).

good. Once again, the scale parameter of the Fréchet distribution has been chosen so that the lines cross at the common 0.9 quantile.

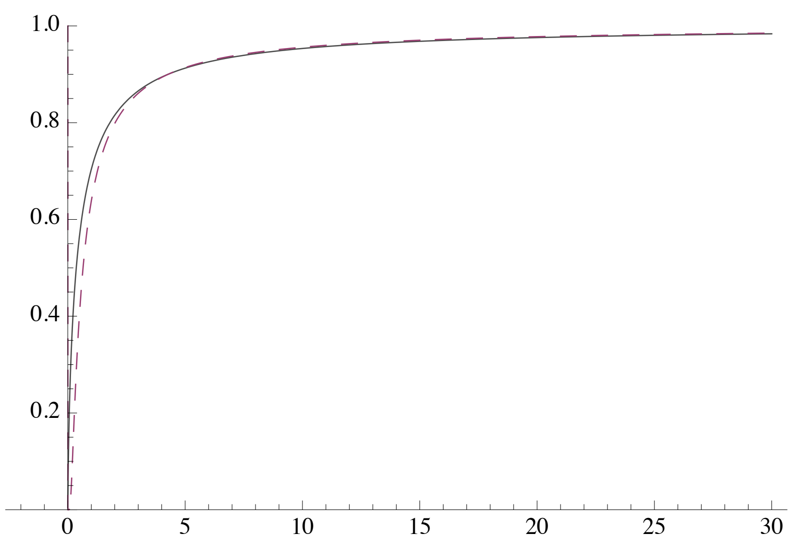

Fig. 10. $2x\,W\left(\frac{1}{2x}\right)\,\mathrm{I}_{(-0,\infty)}(x)$ (solid line) approximation of $\mathrm{e}^{-\frac{0.44995}{x}}\,\mathrm{I}_{(0,\infty)}(x)$ (dashed line).

Below, in Fig. 11, we plot the second derivative of $2x\,W\left(\frac{1}{2x}\right)\,\mathrm{I}_{(-0,\infty)}(x)$. Observe that Mejzler [4], [5], [6], [7], [8] developed an interesting $\mathcal{M}$-class of "self-decomposable" extreme value laws that arise as limit of suitably consistent sequences of independent — but not necessarily identically distributed — random variables, that is in the extreme values scheme a simile of Khinchine's $\mathcal{L}$-class in the asymptotic additive theory. Mejzler's characterization is done in terms of log concavity.

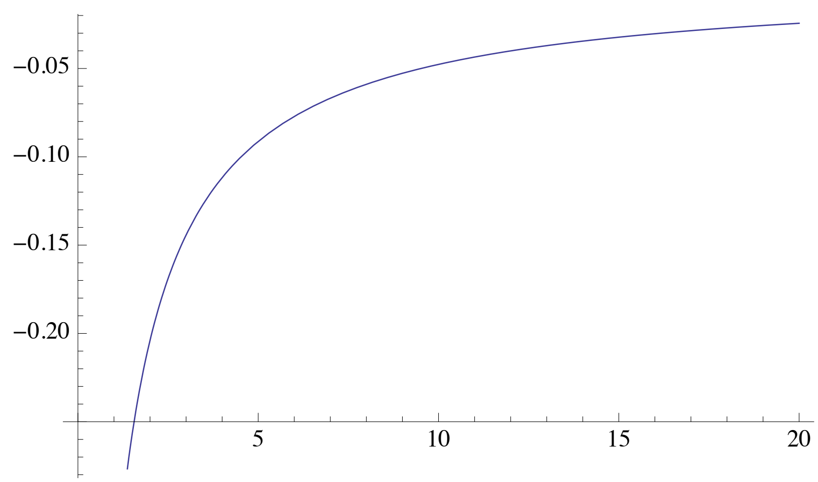

Fig. 11. Log-concavity of $2x\,W\left(\frac{1}{2x}\right)\,\mathrm{I}_{(-0,\infty)}(x)$.

References

1. S. Aleixo, J.L. Rocha, and D. Pestana. Beta(p,q)-Cantor Sets: Determinism and Randomness. In C.H. Skiadas, I. Dimotikalis and C. Skiadas, editors, *Chaos Theory: Modeling, Simulation and Applications*, World Scientific, Singapore, pp. 333–340, 2011.
2. S. Aleixo, J.L. Rocha, and D. Pestana. Populational Growth Model Proportional to Beta Densities. In M.M. Peixoto, A.A. Pinto. and D.A.J. Rand, editors, *Dynamics, Games and Science, in Honour of Mauricio Peixoto and David Rand*, vol II, Ch. 5, pp. 79–95, Springer Verlag, New York 2011.
3. M.F. Brilhante, D. Pestana, and M.L. Rocha. Betices, *Boletim da Sociedade Portuguesa de Matemática*, pp. 177–182, 2011.
4. D. Mejzler. On the problem of the limit distributions for the maximal term of a variational series, *L'vov. Politehn. Inst. Naucn. Zap. Ser. Fiz.-Mat.* vol. 38, pp. 90–109, 1956.
5. D. Mejzler. On a certain class of limit distributions and their domain of attraction. *Trans. Amer. Math. Soc.*, vol. 117, pp. 205–236, 1965.
6. D. Mejzler. Limit distributions for the extreme order statistics. *Can. Math. Bull.*, vol. 21, pp. 447–459, 1978.
7. D. Mejzler. Asymptotic behaviour of the extreme order statistics in the non identically distributed case. In B. Epstein and J. Tiago de Oliveira, eds., *Statistical Extremes and Applications*, 535–547, 1984.

8. D. Mejzler. Extreme value limit laws in the nonidentically distributed case. *Isr. J. Math.*, vol. 57, pp. 1–27, 1987.
9. D. Pestana, S. Aleixo, and J.L. Rocha. Regular variation, paretian distributions, and the interplay of light and heavy tails in the fractality of asymptotic models. In C.H. Skiadas, I. Dimotikalis and C. Skiadas, editors, *Chaos Theory: Modeling, Simulation and Applications*, World Scientific, Singapore, pp. 309–316, 2011.
10. A. Tsoularis. Analysis of logistic growth models. *Res. Lett. Inf. Math. Sci.*, vol. 2, pp. 23–46, 2001.
11. M. E. Turner, E. Bradley, K. Kirk, K. Pruitt. A theory of growth. *Mathematical Biosciences*, vol. 29, pp. 367–373, 1976.

FCT *This reseach has been supported by National Funds through FCT — Fundação para a Ciência e a Tecnologia, project PEst-OE/MAT/UI0006/2011, and PTDC/FEDER.*

Chaotic Modeling and Simulation (CMSIM) 1: 51–59, 2011

Dissipative Solitons: Structural Chaos and Chaos of Destruction

Vladimir L. Kalashnikov

Institute for Photonics, Technical University of Vienna, Vienna, Austria
(E-mail: kalashnikov@tuwien.ac.at)

Abstract. Dissipative soliton, that is a localized and self-preserving structure, develops as a result of two types of balances: self-phase modulation vs. dispersion and dissipation vs. gain. The contribution of dissipative, i.e. environmental, effects causes the complex "far from equilibrium" dynamics of a soliton: it can develop in a localized structure, which behaves chaotically. In this work, the chaotic laser solitons are considered in the framework of the generalized complex nonlinear Ginzburg-Landau model. For the first time to our knowledge, the model of a femtosecond pulse laser taking into account the dynamic gain saturation covering a whole resonator period is analyzed. Two main scenarios of chaotization are revealed: i) multipusing with both short- and long-range forces between the solitons, and ii) noiselike pulse generation resulting from a parametrical interaction of the dissipative soliton with the linear dispersive waves. Both scenarios of chaotization are associated with the resonant and nonresonant interactions with the continuum (i.e. vacuum) excitations.
Keywords: Dissipative soliton, Complex nonlinear Ginzburg-Landau equation, Chaotic soliton dynamics.

1 Introduction

The nonlinear complex Ginzburg-Landau equation (NCGLE) has a lot of applications in quantum optics, modeling of Bose-Einstein condensation, condensate-matter physics, study of non-equilibrium phenomena, and nonlinear dynamics, quantum mechanics of self-organizing dissipative systems, and quantum field theory [1]. In particular, this equation being a generalized form of the so-called master equation provides an adequate description of pulses generated by a mode-locked laser [2]. Such pulses can be treated as the dissipative solitons (DSs), that are the localized solutions of the NCGLE [3]. It was found, that the DS can demonstrate a highly non-trivial dynamics including formation of multi-soliton complexes [4], soliton explosions [5], noise-like solitons [6], etc. The resulting structures can be very complicated and consist of strongly or weakly interacting solitons (so-called soliton molecules and gas) [7] as well as the short-range noise-like oscillations inside a larger wave-packet [8]. The nonlinear dynamics of these structures can cause both regular and chaotic-like behavior.

Received: 20 September 2011 / Accepted: 21 October 2011

ISSN 2241-0503

In this article, the different scenarios of the DS structural chaos will be considered. The first scenario is an appearance of the chaotic fine graining of DS. For such a structure, the mechanism of formation is identified with the parametric instability caused by the resonant interaction of DS with the continuum. The second scenario is formation of the multi-soliton complexes governed by both short-range forces (due to solitons overlapping) and long-range forces (due to gain dynamics). The underlying mechanism of formation is the continuum amplification, which results in the soliton production or/and the dynamical coexistence of DSs with the continuum.

2 Dissipative solitons of the NCGLE

Formally, the NCGLE consists of the nondissipative (hamiltonian) and dissipative parts. The nondissipative part can be obtained from variation of the Lagrangian [9]:

$$\begin{aligned}\mathscr{L} = \frac{i}{2}\left[A^*(x,t)\frac{\partial A(x,t)}{\partial t} - A(x,t)\frac{\partial A^*(x,t)}{\partial t}\right] + \\ +\frac{\beta}{2}\frac{\partial A(x,t)}{\partial t}\frac{\partial A^*(x,t)}{\partial t} - \frac{\gamma}{2}\left|A(x,t)\right|^2,\end{aligned} \tag{1}$$

where $A(x,t)$ is the field envelope depending on the propagation distance x and the "transverse" coordinate t (that is the local time in our case), β is the group-delay dispersion (GDD) coefficient (negative/positive for the normal/anomalous dispersion), and γ is the self-phase modulation (SPM) coefficient [10]. The dissipative part is described by the driving force:

$$\begin{aligned}\mathscr{Q} = -i\mathit{\Gamma} A(x,t) + i\frac{\rho_0}{1+\sigma\int_{-\infty}^{\infty}|A|^2\,dt'}\left[A(x,t) + \tau\frac{\partial^2}{\partial t^2}A(x,t)\right] + \\ +i\kappa\left[|A(x,t)|^2 - \zeta\,|A(x,t)|^4\right]A(x,t),\end{aligned} \tag{2}$$

where $\mathit{\Gamma}$ is the net-dissipation (loss) coefficient, ρ_0 is the saturable gain (σ is the inverse gain saturation energy if the energy E is defined as $E \equiv \int_{-\infty}^{\infty}|A|^2\,dt'$), τ is the parameter of spectral dissipation (so-called squared inverse gainband width), and κ is the parameter of self-amplitude modulation (SAM). The SAM is assumed to be saturable with the corresponding parameter ζ.

Then, the desired CNGLE can be written as

$$\begin{aligned}i\frac{\partial A(x,t)}{\partial x} - \frac{\beta}{2}\frac{\partial^2}{\partial t^2}A(x,t) - \gamma\,|A(x,t)|^2\,A(x,t) = \\ = -i\mathit{\Gamma} A(x,t) + i\frac{\rho_0}{1+\sigma\int_{-\infty}^{\infty}|A|^2\,dt'}\left[A(x,t) + \tau\frac{\partial^2}{\partial t^2}A(x,t)\right] + \\ +i\kappa\left[|A(x,t)|^2 - \zeta\,|A(x,t)|^4\right]A(x,t).\end{aligned} \tag{3}$$

Eq. (3) is not integrable and only sole exact soliton-like solution is known for it [10,11]. Nevertheless, the so-called variational method [9] allows exploring the solitonic sector of (3). The force-driven Lagrange-Euler equations

$$\frac{\partial \int_{-\infty}^{\infty} \mathscr{L} dt}{\partial \mathbf{f}} - \frac{\partial}{\partial x} \frac{\partial \int_{-\infty}^{\infty} \mathscr{L} dt}{\partial \mathbf{f}} = 2\Re \int_{-\infty}^{\infty} \mathscr{Q} \frac{\partial A^*}{\partial \mathbf{f}} dt \tag{4}$$

allow obtaining a set of the ordinary first-order differential equations for a set $\mathbf{f}$ of the soliton parameters if one assumes the soliton shape in the form of some trial function $A(x,t) \approx \mathscr{F}(t, \mathbf{f})$. One may chose [14]

$$\mathscr{F} = a\left(x\right) \operatorname{sech}\left(\frac{t}{T(x)}\right) \exp\left[i\left(\phi(x) + \psi(x) \ln\left(\operatorname{sech}(\frac{t}{T(x)})\right)\right)\right], \tag{5}$$

with $\mathbf{f} = \{a(x), T(x), \phi(x), \psi(x)\}$ describing amplitude, width, phase, and chirp ("squeezing parameter" in other words) of DS, respectively.

Substitution of (5) into (4) results in four equations for the soliton parameters. These equations are completely solvable for a steady-state propagation (i.e. when $\partial_x a = \partial_x T = \partial_x \psi = 0, \partial_x \phi \neq 0$). The analysis demonstrates that the solitonic sector can be completely characterized by two-dimensional master diagram, that is the DS is two-parametrical and the corresponding dimensionless parameters are: $c \equiv \tau\gamma/|\beta|\kappa$, the dimensionless energy is of $\mathscr{E} \equiv E\sqrt{\kappa\zeta/\tau}$ for the anomalous GDD and is of $\mathscr{E} \equiv Eb^{-1}\sqrt{\kappa\zeta/\tau}$ for the normal GDD (here $b \equiv \gamma/\kappa$).

The master diagrams are shown in Fig. 1. The solid curves correspond to the stability thresholds defined as $\mathit{\Gamma} - \rho_0 \Big/ \left(1 + \sigma \int_{-\infty}^{\infty} |A|^2 dt\right) = 0$. Positivity of this value provides the vacuum stability. As will be shown, the vacuum destabilization is main source of the soliton instability causing, in particular, the chaotic dynamics.

The master diagram in Fig. 1, *a* (dashed curve) reveals a very simple asymptotic for the maximum energy of the chirped DS:

$$E \approx 17\,|\beta| \Big/ \sqrt{\kappa\zeta\tau}. \tag{6}$$

The continuum rises above this energy. The corresponding expression for the chirp-free DS developing in the anomalous GDD regime (see dashed curve in Fig. 1, *b*) is

$$E \approx \sqrt{5\beta/\zeta\gamma}. \tag{7}$$

Asymptotical (i.e. corresponding to $c \ll 1$) expressions for the widths of the chirped and chirp-free DSs are:

$$\begin{aligned} T &\approx \frac{8}{|c|}\frac{\gamma}{\kappa}\sqrt{\frac{\tau\zeta}{\kappa}}, \\ T &\approx \frac{2}{\sqrt{5c}}\sqrt{\frac{\tau\zeta}{\kappa}}, \end{aligned} \tag{8}$$

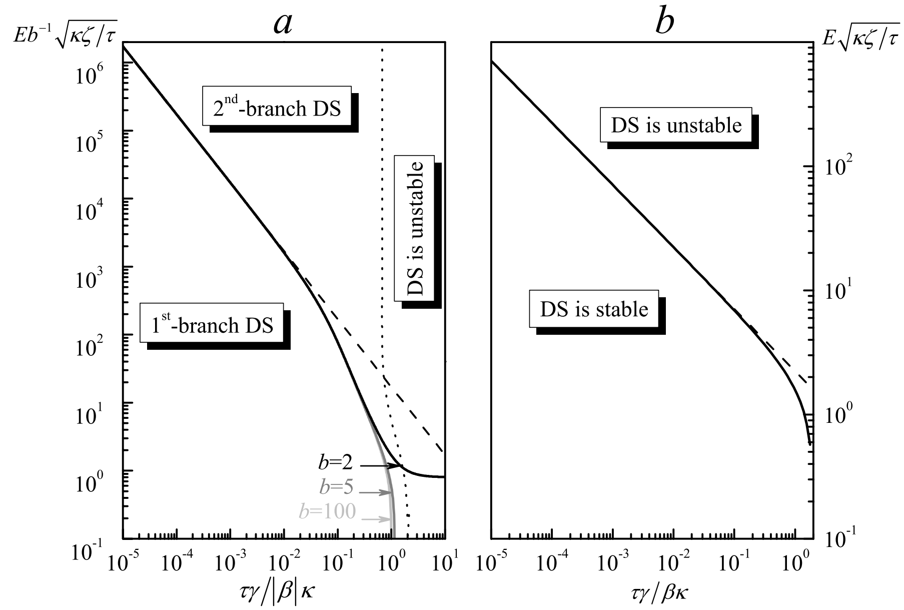

Fig. 1. Master diagrams of DS for the normal (a) and anomalous (b) GDDs. The solid curves correspond to the DS stability thresholds obtained from the variational approximation. The dashed curves correspond to the asymptotic $c \equiv \tau\gamma/|\beta|\kappa \ll 1$. The dotted curve in ($a$) corresponds to the stability threshold of the second DS branch with $\theta > 1$ in (9).

respectively. If the DS in the anomalous GDD is chirp-free by definition, the DS in the normal GDD has an asymptotical chirp $|\psi| \approx 4\kappa/\gamma\,|c|$. One has note, that the asymptotical DS spectral widths are $\propto \sqrt{c\kappa/\tau\zeta}$ for the chirp-free DS and $\propto \sqrt{\kappa/\tau\zeta}$ for the chirped DS.

3 Nonresonant excitation of continuum

The DS of unperturbed Eq. (3) does not interact directly with the continuum. An existence of the stability thresholds shown in Fig. 1 has a simple physical explanation: an approach to the stability threshold causes the DS spectral broadening that increases the spectral loss for the DS [12]. As a result, the DS energy decreases and the energy-dependent net-loss $\Gamma - \rho_0 \Big/ \left(1 + \sigma \int_{-\infty}^{\infty} |A|^2\, dt\right)$ crosses zero-level. Hence, the continuum rises and, in the anomalous GDD regime, the multiple-pulsing develops (Fig. 2, left). Strong interactions inside a multi-pulse complex lead to the structural chaotization. The field remains localized on a picosecond scale, but chaotically structured on a femtosecond one (Fig. 2, right). On the other hand, the solitonic "soup" (Fig. 2, right) can create spontaneously the stable soliton complexes (Fig. 3).

However in the normal GDD, the chirped DS is so adaptable that the spectral loss growth with an approaching to the stability threshold leads to an

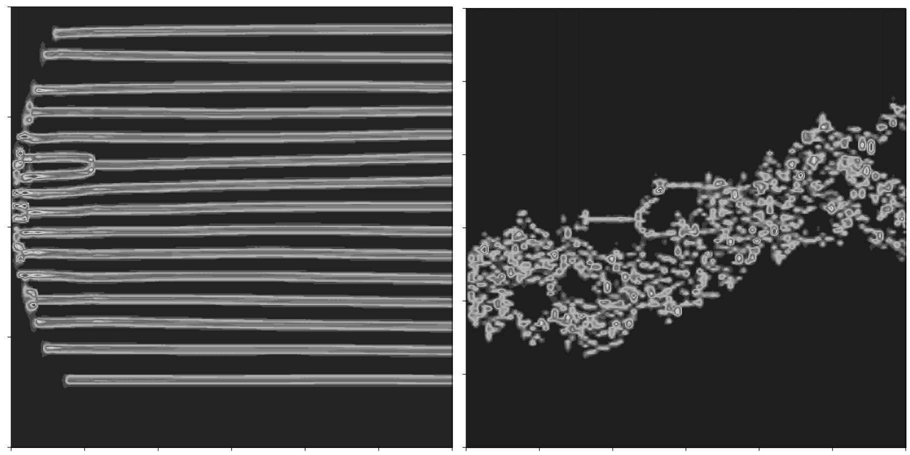

Fig. 2. Multiple-pulse complexes (contour plot with brighter regions corresponding to higher powers) in the anomalous GDD regime. Regular multi-pulsing (left) and structural chaotization (right) with approaching the GDD to zero are shown. The axes are t (vertical) and z (horizontal).

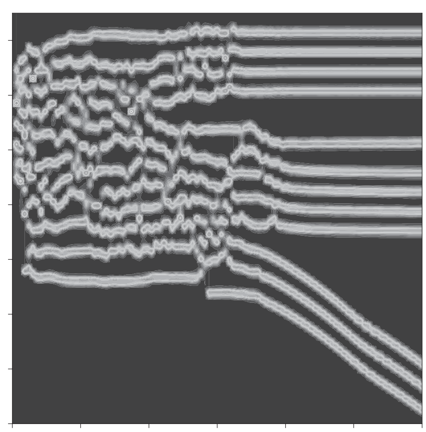

Fig. 3. Spontaneous self-ordering from a solitonic "soup".

appearance of a new DS branch. The stability border corresponding to this branch can be found from the approximated theory of [15] and is shown by the dotted curve in Fig. 1, *a*. Such a branch corresponds to the DS with a so-called "finger-like" spectrum [13,15]. This spectrum has a main part of power in the vicinity of the spectrum center. As a result, a spectral loss decreases that leads to an energy growth close to the boundary of the DS stability. Such a chirped DS provides a perfect energy scalability (dotted curve in Fig. 1, *a*) with $E \xrightarrow{c \to const} \infty$ and can be described by

$$\mathscr{F} = \frac{a(x)}{\sqrt{\theta(x) + \cosh\left(\frac{t}{T(x)}\right)}} \exp\left[i\left(\phi(x) + \psi(x)\ln\left(\theta(x) + \cosh\left(\frac{t}{T(x)}\right)\right)\right)\right] \tag{9}$$

with $\theta(x) > 1$.

An additional source of the DS destabilization is a long range "force" caused by the dynamic gain saturation:

$$\frac{\partial\rho}{\partial t} = P(\rho_0 - \rho) - \sigma\rho|a|^2 - \frac{\rho}{T_r}. \tag{10}$$

Here ρ is the time-dependent gain, P is the pump-rate, and T_r is the gain relaxation time.

The gain dynamics can result in the nonresonant vacuum excitation far from the DS. As a result, a large-scale solitonic (multi-soliton) structure appears (Fig. 4) and, the satellites appear both nearby (few picosecond) the main pulse and far (nanoseconds) from it. Strong interaction between the pulses with the contribution from a gain dynamics results in a chaotic behavior. For the chirped DS, the dynamic gain saturation can result in a parametric resonance and the DS becomes finely structured [18].

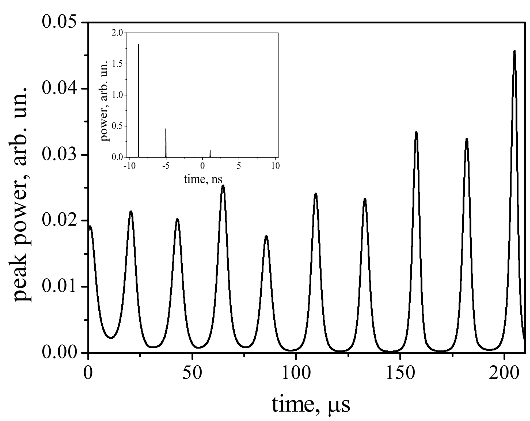

Fig. 4. Multiple DS evolution in the presence of the dynamic gain saturation.

4 Resonant excitation of continuum

The stability threshold shown in Fig. 1 corresponds to an unperturbed DS of (3). The physically meaningful perturbation results from a higher-order dispersion correction to the Lagrangian: $\mathscr{L} = \mathscr{L}_0 + \frac{i\delta}{2}\frac{\partial^2 A}{\partial t^2}\frac{\partial A^*}{\partial t}$, where $\mathscr{L}_0$ is the unperturbed Lagrangian (1) and δ is the third-order dispersion (TOD) parameter. As a result of such perturbation, the resonant interaction of DS with the continuum at some frequency ω_r can appear [16]. The resonance appears if the wave-number of a linear wave (i.e. a vacuum excitation) equals to the DS wave-number q: $\beta\omega^2 + \delta\omega^3 = q$.

Hence, the stability threshold becomes lower (i.e. shifts in the direction of lower E and c) than that shown in Fig. 1. As the resonance occurs in the spectral domain, an exploration of the DS spectrum is most informative in this case. The numerical results corresponding to a mode-locked Cr:ZnSe oscillator [17] are shown in Fig. 5. Non-zero δ can be treated as a frequency-dependence of net-GDD. As a result of such dependence, the zero GDD shifts towards the DS spectrum with the growing $|\delta|$. Increasing TOD transforms the initially rectangular spectrum (curve 1 in Fig. 5) to trapezoid (curve 2) and then to triangular (curve 3) ones. Simultaneously, an dispersive spectral component appears within the anomalous GDD region. The DS spectrum acquires a strong modulation (curve 4), when the resonant frequency shift inside the DS spectrum: $|\omega_r| < \sqrt{\zeta a_0^2/|\beta|} \approx |\beta/\delta|$. Finally, the spectrum becomes completely fragmented with a further TOD growth.

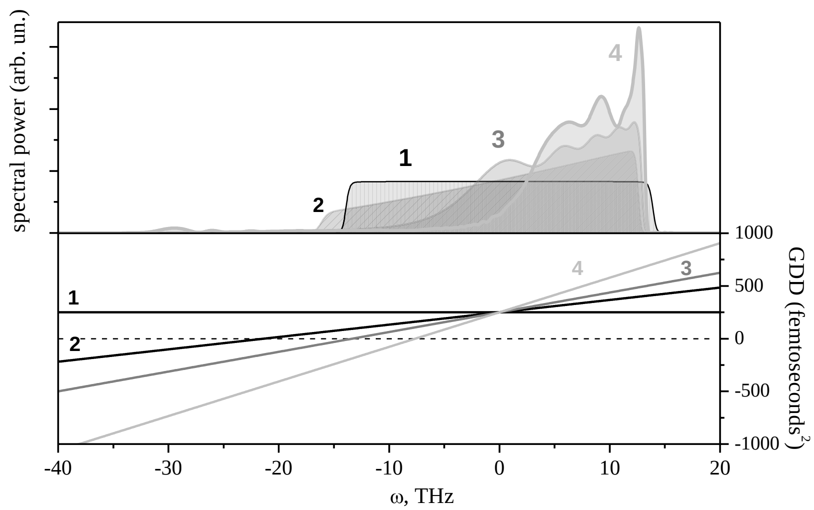

Fig. 5. Spectra of the chirped DSs corresponding to the different net-GDD. The GDD slope depends on the TOD value. Here, the positive GDDs correspond to the normal dispersions.

Resonant interaction with the dispersive wave perturbs strongly the DS spectrum, causes the spectrum structurization and the central frequency jitter. As a result, the soliton behaves chaotically (Fig. 6) although its energy remains almost constant.

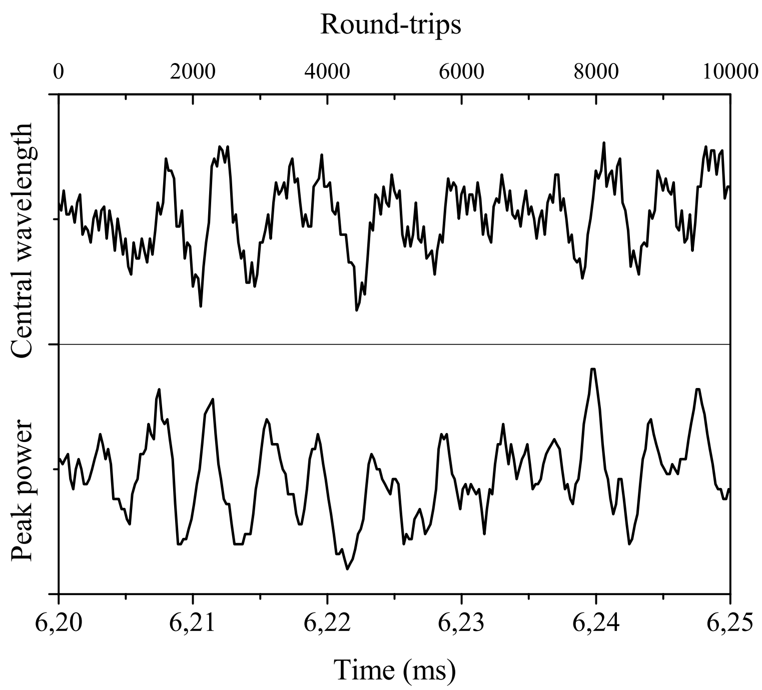

Fig. 6. Jitter of the DS central frequency and its peak power due to resonant interaction with the continuum.

5 Conclusion

Unlike a classical soliton, a DS posses nontrivial dynamics, which can be very complicated. In particular, a chaotic interaction with the excited vacuum (continuum) develops. Such an interaction can be both nonresonant and resonant. A nonresonant excitation of the vacuum forms the multi-soliton complexes. Strong interactions inside such complexes cause the structural chaos. Long-range interactions in a system can be additional source of the nonresonant vacuum excitation that leads to the macro-structural solitonic chaos. A resonant excitation of the vacuum causes the DS spectral jitter with a subsequent chaotic dynamics and even a soliton destruction. One has to note, that a strong localization of the chirped DS does not prevent the soliton traceability in an even chaotic regime. Such a traceability promises a lot of applications in the spectroscopy, for instance.

Acknowledgements

I would like to acknowledge E.Sorokin for his decisive contribution to an investigation of the resonant perturbations of DSs. This work was supported by the Austrian Science Foundation (FWF project P20293).

References

1. I.S. Aranson, L. Kramer. The world of the complex Ginzburg-Landau equation. *Rev. Mod. Phys.*, 74:99–143, 2002.
2. F.X. Kärtner, U. Morgner, Th. Schibli, R. Ell, H.A. Haus, J.G. Fujimoto, E.P. Ippen. Few-cycle pulses directly from a laser. In F.X. Kärtner, editor, *Few-cycle Laser Pulse Generation and its Applications*, pages 73-178, Berlin, 2004. Springer.
3. N. Akhmediev, A. Ankiewicz. Dissipative solitons in the complex Ginzburg-Landau and Swift-Hohenberg equations. In N. Akhmediev, A. Ankiewicz, editors, *Dissipative Solitons*, pages 1–18, Berlin, 2005. Springer.
4. J.M. Soto-Crespo, Ph. Grelu. Temporal multi-soliton complexes generated by passively mode-locked lasers. In N. Akhmediev, A. Ankiewicz, editors, *Dissipative Solitons*, pages 207–240, Berlin, 2005. Springer.
5. S.T. Cundiff. Soliton dynamics in mode-locked lasers. In N. Akhmediev, A. Ankiewicz, editors, *Dissipative Solitons*, pages 183–206, Berlin, 2005. Springer.
6. M. Horowitz, Y. Barad, Y. Silberberg. Noiselike pulses with a broadband spectrum generated from an erbium-doped fiber laser. *Opt. Letters*, 22:799–801, 1997.
7. A. Zavyalov, R. Iliew, O. Egorov, F. Lederer. Dissipative soliton molecules with independenly evolving or flipping phases in mode-locked fiber lasers. *Phys. Rev. A*, 80:043829, 2009.
8. S. Kobtsev, S. Kukarin, S. Smirnov, S. Turitsyn, A. Latkin. Generation of double-scale femto/pico-second optical lumps in mode-locked fiber lasers. *Optics Express*, 17:20707–20713, 2009.
9. D. Anderson, M. Lisak, and A. Berntson. A variational approach to nonlinear equations in optics. *Pramana J. Phys.* 57:917-936, 2001.
10. N. Akhmediev, A. Ankiewicz. *Solitons: Nonlinear Pulses and Beams*, London, 1997. Chapman&Hall.
11. R. Conte, M. Musette. Solitary waves of nonlinear nonintegrable equations. In N. Akhmediev, A. Ankiewicz, editors, *Dissipative Solitons*, pages 373–406, Berlin, 2005. Springer.
12. V.L. Kalashnikov, E. Sorokin, I.T. Sorokina. Multipulse operation and limits of the Kerr-lens mode-locking stability. *IEEE J. Quantum Electron.*, 39:323–336, 2003.
13. V.L. Kalashnikov. Chirped dissipative solitons. In L.F. Babichev, V.I.Kuvshinov, editors, *Nonlinear Dynamics and Applications*, pages 58–67, Minsk, 2010. Republican Institute of higher school.
14. V.L. Kalashnikov, A. Apolonski. Energy scalability of mode-locked oscillators: a completely analytical approach to analysis. *Optics Express*, 18:25757–25770, 2010.
15. E. Podivilov, V.L. Kalashnikov. Heavily-chirped solitary pulses in the normal dispersion region: new solutions of the cubic-quintic complex Ginzburg-Landau equation. *JETP Letters*, 82:467–471, 2005.
16. V.L. Kalashnikov. Dissipative solitons: perturbations and chaos formation. In *Proceedings of 3nd Chaotic Modeling and Simulation International Conference*, pages 69-1–8. 1-4 June, 2010, Chania, Greece.
17. V.L. Kalashnikov, E. Sorokin. Soliton absorption spectroscopy. *Phys. Rev. A*, 81:033840-1–8, 2010.
18. V.L. Kalashnikov. Chirped-pulse oscillators: an impact of the dynamic gain saturation. arXiv:0807.1050 [physics.optics].